


**Electrostatic Ion Cyclotron Waves in Barium Injection**


**Experiments in Space**

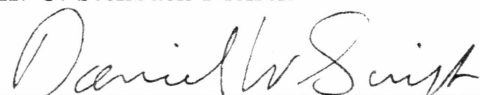
by

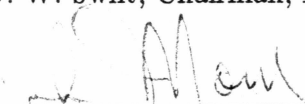
Kim A. Kangas

RECOMMENDED:

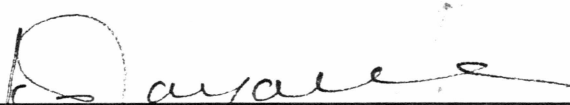
  
\_\_\_\_\_  
J. R. Kan

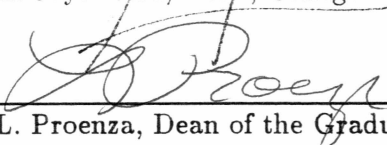
  
\_\_\_\_\_  
H. C. Stenbaek-Nielsen

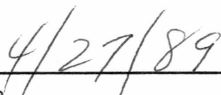
  
\_\_\_\_\_  
D. W. Swift, Chairman, Advisory Committee

  
\_\_\_\_\_  
J. L. Morack, Head, Physics Department

APPROVED:

  
\_\_\_\_\_  
K. Jayaweera, Dean, College of Natural Sciences

  
\_\_\_\_\_  
L. Proenza, Dean of the Graduate School

  
\_\_\_\_\_  
Date

**" ELECTROSTATIC ION CYCLOTRON WAVES IN BARIUM INJECTION  
EXPERIMENTS IN SPACE"**

A  
THESIS

Presented to the Faculty of the University of Alaska  
in Partial Fulfillment of the Requirements  
for the Degree of

MASTER OF SCIENCE

By  
Kim A. Kangas, B. S.

Fairbanks, Alaska

May 1989

**RASMUSON LIBRARY**  
UNIVERSITY OF ALASKA-FAIRBANKS

QC  
809  
P5  
K36  
1989



## ABSTRACT

Electrostatic ion cyclotron waves are investigated in a charge-generated barium-shaped plasma directed parallel to the earth's magnetic field. The barium plasma is generated as a result of a barium shape charge release in the upper  $F_2$  region of the ionosphere undergoing photoionization. Using a differential velocity distribution given by Stenbaek-Nielsen et al., [1984], this situation has been modeled based on the condition of collisionless plasma. The instabilities were studied for cases with and without an ambient oxygen ion background. It was concluded that fast ionization in excess of photoionization due to the excitation of electrons by electrostatic ion cyclotron waves was not feasible for the ejection directed along the earth's magnetic field nor would there be any contribution to Alfvén's critical velocity mechanism if the injection was directed perpendicular to the magnetic field.

## Table of Contents

	page
Abstract .....	iii
List of figures .....	v
Acknowledgments .....	vii
<b>Chapter 1: Introduction</b> .....	<b>1</b>
<b>Chapter 2: Derivation of the Neutral Barium and Barium Ion Densities</b> ....	<b>4</b>
2.1 Number Density of the Neutral Barium Atoms .....	4
2.2 Calculation of the Barium Ion Velocity Distribution and Density .....	7
2.3 Calculations and Results of Number Densities .....	13
<b>Chapter 3: Derivation of the Dispersion Relation</b> .....	<b>16</b>
<b>Chapter 4: Calculation of the Dispersion Relation for a Particular Model</b> .	<b>28</b>
4.1 Parameters .....	28
4.2 No Ambient Plasma .....	31
4.3 Effects of Ambient Plasma .....	33
<b>Chapter 5: Conclusions</b> .....	<b>49</b>
References .....	57

## List of Figures

	Page
Figure 1: Distribution of the number of particles associated with velocity.	8
Figure 2: Number density contours of the barium atoms at times 1, 2, 5, and 10 seconds after detonation.	14
Figure 3: Number density contours of the barium ions at the same conditions as in Fig.2.	15
Figure 4: Distribution of barium ions associated with velocity for a position of $z = 5km$ , $\rho = 1km$ , and a time of 1 second after detonation.	19
Figure 5: Zero frequency instabilities, perpendicular to the magnetic field, for the case with no ambient oxygen ion background.	36
Figure 6a: Plasma instability (electrostatic ion cyclotron waves) corresponding to the first harmonic for the case with no ambient oxygen ion background.	37
Figure 6b: Frequency associated with the first harmonic for the case with no ambient oxygen ion background.	38
Figure 7a: Plasma instability (electrostatic ion cyclotron waves) corresponding to the second harmonic for the case with no ambient oxygen ion background.	39
Figure 7b: Frequency associated with the second harmonic for the case with no ambient oxygen ion background.	40
Figure 8a: Growth rates corresponding to the first harmonic for the case with an ambient oxygen ion background.	41
Figure 8b: Frequency associated with the first harmonic for the case with an ambient oxygen ion background.	42
Figure 9a: Growth rates corresponding to the second harmonic for the case with an ambient oxygen ion background.	43
Figure 9b: Frequency associated with the second harmonic for the case with an ambient oxygen ion background.	44

Figure 10a: Growth rates corresponding to the third harmonic for the case with an ambient oxygen ion background.	45
Figure 10b: Frequency associated with the third harmonic for the case with an ambient oxygen ion background.	46
Figure 11a: Growth rates corresponding to the fourth harmonic for the case with an ambient oxygen ion background.	47
Figure 11b: Frequency associated with the fourth harmonic for the case with an ambient oxygen ion background.	48

## Acknowledgments

I would like to express my appreciation for the time, effort, and advice that Dan W. Swift, advisor and chairman of my graduate committee, has given to me in the preparation of this thesis. Also, I wish to thank my thesis committee members, Hans C. Stenbaek-Nielsen and Joe R. Kan, for their helpful advice and comments. Special thanks are extended to John V. Olson who first introduced me to the Geophysical Institute and acted as my advisor for my first year at the University of Alaska.

I wish to extend thanks to all my fellow graduate students and friends, Chris Grimm, Wei Xin, Alan Koivunen, and others for their contributions and warm fellowship.

This research was sponsored by NASA grant NAGW-269.

## Chapter 1: Introduction

Alfven's critical velocity mechanism for the ionization of a neutral gas streaming through a plasma across a magnetic field has been the subject of interest since he first proposed it as part of a process in the formation of the planets [Alfven, 1954]. The mechanism was given further credibility when Danielsson and Brenning, [1975] obtained laboratory evidence to confirm an enhanced ionization that followed Alfven's critical velocity relation

$$v_{cr} = \left( \frac{2e\varphi}{m} \right)^{\frac{1}{2}} \quad (1)$$

where  $v_{cr}$  is the critical velocity,  $m$  the mass,  $e$  the charge, and  $\varphi$  the ionization potential of the particle.

The importance of active space experiments was later pointed out by Mobius, [1983]. He stated that all laboratory experiments differ from astrophysical situations in two basic features besides the scaling of dimensions and plasma parameters. First, in the laboratory the magnetized plasma is always driven by an external electromagnetic force rather than having the free energy available in the neutral gas and second the walls and electrodes are always present thus leading to unsuspected side effects. Efforts were then concentrated to verify Alfven's critical velocity mechanism by active experiments in space.

In 1980, Haerendel carried out an experiment where barium gas, which has a low critical velocity  $v_{cr} = 2.7 km/s$ , was injected into space. The experiment revealed the existence of an enhanced ionization process consistent with the critical velocity mechanism [Haerendel, 1982]. Experiments were then designed to specifically test the critical velocity mechanism in space. In March 1983, two such space experiments the star of Lima [Wescott et al., 1986a] and the star of condor [Wescott et al., 1986b] were carried out. The star of Lima was set

up to inject barium vapor perpendicular to the earth's magnetic field in a conical shaped-charge at an altitude of 430 km. The star of condor injected strontium vapor perpendicular to the earth's magnetic field in a radially shaped-charge at an altitude of 571.11 km. In both experiments the Alfvén process failed to produce an enhanced ionization that was visible from the ground.

It was later noted that the most rapid ionization appeared to take place in releases nearly parallel to the magnetic field [Hallinan, 1985]. But, after more rigorous scrutiny Hallinan notes that the appearance of most jets were found to be consistent with the slow process of photoionization. Some injection experiments did produce a thin confined jet that was suggestive of fast ionization. However, by comparison of intensity profiles through the jet for various assumed time constants, it was determined that the measured profile was consistent with any time constant of photoionization in excess of 20 seconds and was inconsistent with fast ionization in excess of 1% of the barium [Hallinan, 1988].

It has been suggested that a possible mechanism for enhanced ionization could be due to the streaming of the photoionized ions through the plasma leading to the heating of electrons that would cause fast ionization. In 1987, Wei Xin investigated the hypothesis that rapid ionization is caused by electrons heated in an ion cyclotron wave excited by the field-aligned streaming of barium ions through the ambient ionospheric plasma. The model used assumed an ionosphere background plasma with a Maxwellian velocity distribution and a drifting Maxwellian distribution in the direction of the magnetic field to represent the photoionized barium. It was found that electrostatic ion cyclotron wave near the barium ion cyclotron frequency was dominant. It was proposed that the electrons can be heated by the doppler shifted waves via Landau damping of motion parallel to the magnetic field.

The purpose of this study is to include additional information for a revised model of a barium injection for the investigation of electrostatic ion cyclotron waves. This model shall take the injection to be parallel to the magnetic field and use a background of oxygen ions and electrons to represent the ionosphere. Upon injection of the neutral barium vapor a portion will become ionized due to photoionization. This seed population of ions produces a ring type distribution that gives rise to free energy in the system. The free energy is then transferred by plasma waves. In Chapter 2, expressions will be derived for the number density of the injected neutral barium vapor, the barium ion distribution function, and the barium ion number density. Chapter 3 will deal with the derivation of the dispersion equation in which we shall make use of the derived expressions in Chapter 2. In Chapter 4 the roots to the dispersion equation will be shown for specific cases and be discussed. Finally, this thesis ends with an assessment of the likelihood that the ion cyclotron waves excited could lead to anomalous ionization in Chapter 5.



## Chapter 2: Derivation of the Neutral Barium and Barium Ion Number Densities

In this chapter, expressions will be derived for the neutral barium and barium ion number densities caused by the release of barium vapor by a conical shaped charge directed at small angles to the earth's magnetic field in the ionosphere. The barium shaped charge is an explosive device lined with barium metal. The geometry of the device is such that when detonated it projects the barium in a particular direction which we shall refer to as the burst direction [Stenbaek-Nielsen et al., 1984].

### 2.1 Number Density of the Neutral Barium Atoms

It is assumed that the neutrals are release from a point at time  $t = 0$ . The particles then follow straight-line trajectories, traveling radially outward from the shaped charge explosion. Also, we assume there are no collisions with ambient particles . The neutral density will be calculated from the differential velocity distribution

$$\eta = \frac{d^2 N}{dv d\theta} \quad (2.1)$$

which is the number of particles with speeds  $v$  and  $v+dv$  and with polar angles  $\theta$  and  $\theta+ d\theta$ , where  $\theta$  is the angle between the axis of the conical burst direction and the radial vector. Rotational symmetry is assumed about the burst direction. Specifically we assume

$$\eta = \mu N F(v) \exp \left[ -\frac{\theta^2}{\Theta^2} \right] \quad (2.2)$$

where  $N$  is the total number of neutral particles injected;  $\mu$  is a normalizing constant, and  $\Theta$  the angular width of the burst which is taken to be  $15^\circ$ . The velocity distribution,  $F(v)$ , was taken from television observations of an ion jet and has been given by Wescott et al., [1975b], and Stenbaek-Nielsen et al., [1984].

The neutral barium number density is

$$n_n = \frac{\Delta N}{\Delta V} \quad (2.3)$$

where  $\Delta N$  and  $\Delta V$  are incremental changes in the number of neutrals and the volume, respectively. We can obtain an expression for  $\Delta N$  by multiplying  $\eta$  with a small change in spherical velocity space

$$\Delta N = \eta 2\pi \sin \theta \Delta \theta \Delta v \quad (2.4)$$

where  $\Delta v$  and  $\Delta \theta$  are incremental changes in velocity and polar angle  $\theta$ . Using the assumption that the distribution started from a point at  $t = 0$ , we get a relationship between the velocity and the distance from the release point

$$v = \frac{r}{t}$$

and thus for a small change in distance

$$\Delta r = t \Delta v$$

The incremental volume is described by

$$\Delta V = \Delta A t \Delta v \quad (2.5)$$

where  $\Delta A$  is a small element of area. Since there is azimuthal symmetry,  $\Delta A$  in spherical coordinates becomes

$$\Delta A = 2\pi r^2 \sin \theta \Delta \theta \quad (2.6)$$

Substituting this into eqn(2.5)

$$\Delta V = r^2 t 2\pi \sin \theta \Delta v \Delta \theta \quad (2.7)$$

Now with the substitution of eqn(2.4) and eqn(2.7) into eqn (2.3) the neutral number density becomes

$$n_n = \frac{\Delta N}{\Delta V} = \frac{\eta 2\pi \sin \theta \Delta v \Delta \theta}{r^2 t 2\pi \sin \theta \Delta v \Delta \theta} \quad (2.8)$$

and thus

$$n_n = \frac{\eta}{r^2 t} \quad (2.9)$$

It can be seen that  $r^2$  comes from the conservation of flux and that  $t$  is a dispersion term for the velocity.

In dealing with the derivation of  $n_n$  we have not included the loss of neutral barium by photoionization. Photoionization will cause a fraction of the barium neutrals to be ionized after a certain amount of time and then a fraction of the atoms not previously ionized will be ionized. This continues until all the barium atoms are ionized. Thus, we take the photoionization of the neutrals to be described by an exponential decay. Including this into the neutral barium number density we have

$$n_n = \frac{\eta}{r^2 t} \exp \left[ -\frac{t}{\tau_o} \right] \quad (2.10)$$

where the exponential represents the loss of neutrals to photoionization and  $\tau_o$  is the photoionization lifetime. Substituting eqn(2.2) into eqn(2.10) we obtain

$$n_n = \frac{1}{r^2 t} \mu N F(v) \Big|_{v=\frac{r}{t}} \exp \left[ -\frac{\theta^2}{\Theta^2} \right] \exp \left[ -\frac{t}{\tau_o} \right] \quad (2.11)$$

which we write as

$$n_n = \frac{1}{r^2 t} f \left( \frac{r}{t} \right) \exp \left[ -\frac{\theta^2}{\Theta^2} \right] \exp \left[ -\frac{t}{\tau_o} \right] \quad (2.12)$$

where  $f\left(\frac{r}{t}\right) = \mu N F(v)$  was obtained from Stenbaek-Nielsen et al. ,1984 and is plotted in Fig.1.

## 2.2 Calculation of Barium Ion Velocity Distribution and Density

The calculation of the barium ion distribution and density assumes that barium ions are created by photoionization of the injected barium neutrals. Once an ion is created, its motion is constrained by the magnetic field. Its velocity along the magnetic field stays constant while its perpendicular velocity with respect to the magnetic field causes cyclotron motion. We assume there is no electric field present and effects of gravity are negligible. Thus the ion behavior may be described in terms of a distribution function  $f_{Ba_0}(\mathbf{x}, \mathbf{v}, t)$  that satisfies the equation

$$\frac{\partial f_{Ba_0}}{\partial t} + \mathbf{v} \cdot \frac{\partial f_{Ba_0}}{\partial \mathbf{x}} + (\mathbf{v} \times \boldsymbol{\Omega}) \cdot \frac{\partial f_{Ba_0}}{\partial \mathbf{v}} = \frac{1}{\tau_0} n_n \delta^3\left(\mathbf{v} - \frac{\mathbf{x}}{t}\right) \quad (2.13)$$

where  $\boldsymbol{\Omega}$ , the cyclotron frequency, is in the direction of the magnetic field. This states that the total time derivative for the ions with velocity  $\mathbf{v}$  is given by the rate of decay of the neutrals present in a given volume element.

Since we assumed radial symmetry for the injection of the barium we wish to solve for the zero order barium distribution function in cylindrical velocity and configuration space coordinates. This should help simplify our expressions. The transformation from cartesian to cylindrical coordinates are

$$\begin{aligned} z &= z & x &= \rho \cos \phi & y &= \rho \sin \phi \\ v_z &= v_{\parallel} & v_x &= v_{\perp} \cos \psi & v_y &= v_{\perp} \sin \psi \\ \rho &= (x^2 + y^2)^{\frac{1}{2}} & v_{\perp} &= (v_x^2 + v_y^2)^{\frac{1}{2}} \end{aligned} \quad (2.14)$$

## VELOCITY DISTRIBUTION FOR THE BARIUM

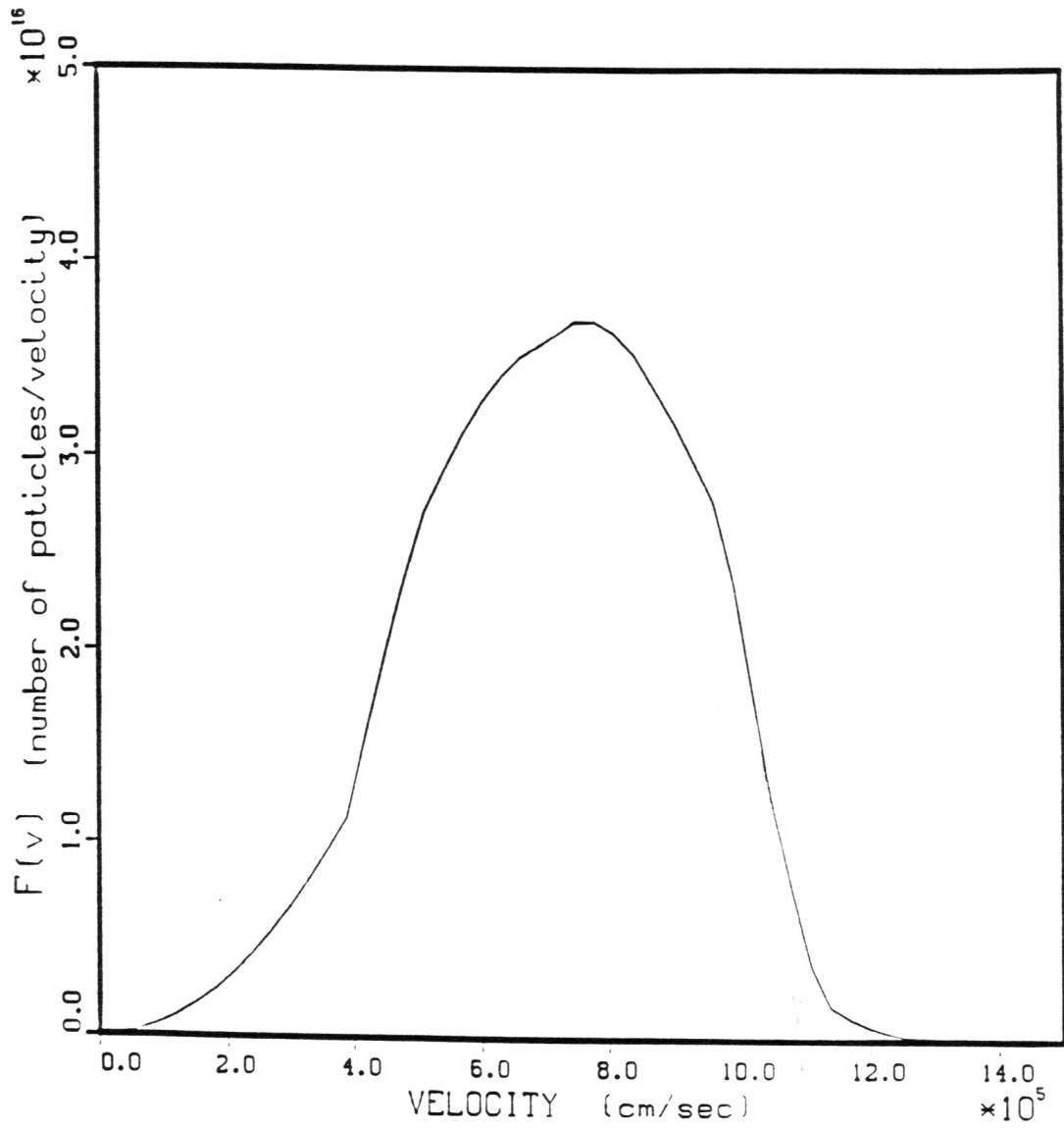


Figure 1: Distribution of the number of particles associated with velocity

where  $z$  and  $v_z$  are the magnitudes of the vectors along the magnetic field,  $\rho$  is the magnitude of the vector perpendicular to the magnetic field,  $\phi$  the angle between  $\rho$  and  $x$ , and  $\psi$  the angle between  $v_\perp$  and  $v_x$ . Also, the angles  $\psi$  and  $\phi$  are related by a phase difference. The transformation from the coordinates of  $n_n$  to those just mentioned depends on the direction of the burst relative to the magnetic field. Since the axis of the burst is along the magnetic field, we take it to be in the  $z$  direction. The transformations from spherical to the above cylindrical coordinates for  $n_n$  are

$$r = \sqrt{\rho^2 + z^2}$$

$$\tan \theta = \frac{\rho}{z} \quad (2.15)$$

We now proceed with the transformation of the third term on the left hand side of equation (2.13) into cylindrical coordinates. Since we took the magnetic field to be in the  $z$  direction, the third term can be written as

$$(\mathbf{v} \times \boldsymbol{\Omega}) \cdot \frac{\partial f_{B a_0}}{\partial \mathbf{v}} = \Omega \left( v_y \frac{\partial}{\partial v_x} - v_x \frac{\partial}{\partial v_y} \right) f_{B a_0} \quad (2.16)$$

where  $\boldsymbol{\Omega}$  is in the  $z$  direction. The transformations of  $\frac{\partial}{\partial v_x}$  and  $\frac{\partial}{\partial v_y}$  are accomplished by making use of the chain rule. Since  $v_x$  and  $v_y$  are functions of  $v_\perp$  and  $\psi$  we have

$$\frac{\partial}{\partial v_x} = \frac{\partial \psi}{\partial v_x} \frac{\partial}{\partial \psi} + \frac{\partial v_\perp}{\partial v_x} \frac{\partial}{\partial v_\perp} \quad (2.17)$$

$$\frac{\partial}{\partial v_y} = \frac{\partial \psi}{\partial v_y} \frac{\partial}{\partial \psi} + \frac{\partial v_\perp}{\partial v_y} \frac{\partial}{\partial v_\perp} \quad (2.18)$$

and we determine from the transformations that

$$\frac{\partial v_\perp}{\partial v_x} = \frac{v_x}{v_\perp} = \cos \psi$$

$$\frac{\partial v_\perp}{\partial v_y} = \frac{v_y}{v_\perp} = \sin \psi \quad (2.19)$$

$$\tan \psi = \frac{v_y}{v_x}$$

We may get expressions for  $\partial\psi/\partial v_x$  and  $\partial\psi/\partial v_y$  by taking the derivative of the  $\tan \psi$  with respect to  $v_x$  and  $v_y$  and employing the chain rule

$$\begin{aligned} \frac{\partial\psi}{\partial v_x} \frac{\partial}{\partial\psi} (\tan \psi) &= \frac{\partial\psi}{\partial v_x} \frac{\partial}{\partial\psi} \left( \frac{v_y}{v_x} \right) \\ \frac{\partial\psi}{\partial v_x} \sec^2 \psi &= \frac{\partial}{\partial v_x} \left( \frac{v_y}{v_x} \right) \\ \frac{\partial\psi}{\partial v_x} \sec^2 \psi &= -\frac{v_y}{v_x^2} \\ \frac{\partial\psi}{\partial v_x} &= -\frac{v_y}{v_x^2} \cos^2 \psi \end{aligned} \tag{2.20}$$

With the substituting from the transformations of  $v_x$  and  $v_y$  we get

$$\frac{\partial\psi}{\partial v_x} = -\frac{1}{v_\perp} \sin \psi \tag{2.21}$$

and by the same means we have

$$\frac{\partial\psi}{\partial v_y} = \frac{1}{v_\perp} \cos \psi \tag{2.22}$$

Substituting equations (2.17), (2.18), and the appropriate transformations into eqn (2.16) we get

$$\begin{aligned} (\mathbf{v} \times \boldsymbol{\Omega}) \cdot \frac{\partial f_{B^{a_0}}}{\partial \mathbf{v}} &= \Omega \left[ v_\perp \sin \psi \left( \frac{\partial\psi}{\partial v_x} \frac{\partial}{\partial\psi} + \frac{\partial v_\perp}{\partial v_x} \frac{\partial}{\partial v_\perp} \right) \right. \\ &\quad \left. - v_\perp \cos \psi \left( \frac{\partial\psi}{\partial v_y} \frac{\partial}{\partial\psi} + \frac{\partial v_\perp}{\partial v_y} \frac{\partial}{\partial v_\perp} \right) \right] f_{B^{a_0}} \end{aligned} \tag{2.23}$$

which by rearranging we have

$$\begin{aligned} (\mathbf{v} \times \boldsymbol{\Omega}) \frac{\partial f_{B^{a_0}}}{\partial \mathbf{v}} &= \Omega \left[ v_\perp \left( \sin \psi \frac{\partial\psi}{\partial v_x} - \cos \psi \frac{\partial\psi}{\partial v_y} \right) \frac{\partial}{\partial\psi} \right. \\ &\quad \left. + v_\perp \left( \sin \psi \frac{\partial v_\perp}{\partial v_x} - \cos \psi \frac{\partial v_\perp}{\partial v_y} \right) \frac{\partial}{\partial v_\perp} \right] f_{B^{a_0}} \end{aligned} \tag{2.24}$$

and with the substitutions of equations (2.19), (2.21), and (2.22) we arrive at

$$(\mathbf{v} \times \boldsymbol{\Omega}) \frac{\partial f_{Ba_0}}{\partial \mathbf{v}} = \Omega \left[ (\sin^2 \psi + \cos^2 \psi) \frac{\partial}{\partial \psi} + v_{\perp} (\sin \psi \cos \psi - \cos \psi \sin \psi) \frac{\partial}{\partial v_{\perp}} \right] f_{Ba_0}$$

$$(\mathbf{v} \times \boldsymbol{\Omega}) \frac{\partial f_{Ba_0}}{\partial \mathbf{v}} = -\Omega \frac{\partial f_{Ba_0}}{\partial \psi} \quad (2.25)$$

The equation for the zero order distribution function is

$$\frac{\partial f_{Ba_0}}{\partial t} + v_{\perp} \cos \psi \frac{\partial f_{Ba_0}}{\partial x} + v_{\perp} \sin \psi \frac{\partial f_{Ba_0}}{\partial y} + v_{\parallel} \frac{\partial f_{Ba_0}}{\partial z} - \Omega \frac{\partial f_{Ba_0}}{\partial \psi}$$

$$= \frac{1}{2\pi\tau_0} n_n(z, \rho, t) \delta\left(v_{\parallel} - \frac{z}{t}\right) \frac{1}{v_{\perp}} \delta\left(v_{\perp} - \frac{\rho}{t}\right) \delta(\psi - \phi) \quad (2.26)$$

Now, with the assumption that the distribution is not affected by the particles' gyromotion, we take  $\partial f_{Ba_0}/\partial x$  and  $\partial f_{Ba_0}/\partial y$  to be independent of  $\psi$ . Averaging over  $\psi$  we have

$$\frac{\partial f_{Ba_0}}{\partial t} + v_{\parallel} \frac{\partial f_{Ba_0}}{\partial z} = \frac{1}{2\pi\tau_0} n_n(z, \rho, t) \delta\left(v_{\parallel} - \frac{z}{t}\right) \frac{1}{v_{\perp}} \delta\left(v_{\perp} - \frac{\rho}{t}\right) \quad (2.27)$$

The left side of the above equation is a total derivative along a straight-line trajectory. The solution is therefore given by the integral expression

$$f_{Ba_0} = \frac{1}{2\pi\tau_0} \int_0^t dt' n_n(z', \rho', t') \delta\left(v_{\parallel} - \frac{z'}{t'}\right) \frac{1}{v_{\perp}} \delta\left(v_{\perp} - \frac{\rho'}{t'}\right) \quad (2.28)$$

where

$$z' = z - v_{\parallel} (t - t') \quad (2.29)$$

$$\rho' = \rho$$

The implicit assumption is that the gyroradius is small compared to  $\rho$ .

The barium ion number density is found by integrating the zero order distribution function,  $f_{Ba_0}$ , over velocity space

$$n_{Ba_0} = \int d^3v f_{Ba_0}$$



$$n_{Ba_0} = \frac{1}{2\pi\tau_0} \int_0^t dt' \int 2\pi v_\perp dv_\perp \int dv_\parallel n_n(z', \rho', t') \frac{1}{v_\perp} \delta\left(v_\perp - \frac{\rho'}{t'}\right) \delta\left(v_\parallel - \frac{z'}{t'}\right) \quad (2.30)$$

With the substitutions for  $z'$  and  $\rho'$  the delta functions become

$$\begin{aligned} \delta\left(v_\parallel - \frac{z'}{t'}\right) &= \delta\left(v_\parallel - \frac{(z - v_\parallel(t - t'))}{t'}\right) \\ &= \delta\left(\frac{t}{t'}\left(v_\parallel - \frac{z}{t}\right)\right) \\ &= \frac{t'}{t} \delta\left(v_\parallel - \frac{z}{t}\right) \end{aligned} \quad (2.31)$$

and

$$\delta\left(v_\perp - \frac{\rho'}{t'}\right) = \delta\left(v_\perp - \frac{\rho}{t'}\right) \quad (2.32)$$

putting these back into  $n_{Ba_0}$  we obtain

$$\begin{aligned} n_{Ba_0} &= \frac{1}{\tau_0} \int_0^t dt' \int dv_\perp \int dv_\parallel \frac{t'}{t} n_n(z - v_\parallel(t - t'), \rho, t') \delta\left(v_\perp - \frac{\rho}{t'}\right) \delta\left(v_\parallel - \frac{z}{t}\right) \\ &= \frac{1}{\tau_0} \int_0^t dt' \int dv_\perp \frac{t'}{t} n_n\left(\frac{z}{t}, \rho, t'\right) \delta\left(v_\perp - \frac{\rho}{t'}\right) \\ &= \frac{1}{\tau_0} \int_0^t dt' \frac{t'}{t} n_n\left(\frac{z}{t}, \rho, t'\right) \end{aligned} \quad (2.33)$$

Now substituting in  $n_n$  we have

$$n_{Ba_0} = \frac{1}{\tau_0} \int_0^t dt' \frac{t'}{t} \frac{f\left(\frac{r'}{t'}\right)}{r'^2 t'} \exp\left[-\frac{\theta'^2}{\Theta^2}\right] \exp\left[-\frac{t'}{\tau_0}\right] \quad (3.34)$$

since

$$\begin{aligned} r'^2 &= \rho'^2 + z'^2 \\ &= \rho^2 + \frac{z^2 t'^2}{t^2} \end{aligned}$$

and

$$\tan \theta' = \frac{\rho'}{z'}$$

which for small  $\theta'$

$$\theta' = \frac{\rho'}{z'} = \frac{\rho}{\frac{zt'}{t}} = \frac{\rho t}{zt'}$$

the barium ion number density is described by

$$n_{Ba_0} = \frac{1}{\tau_0 t} \int_0^t dt' \frac{f\left(\sqrt{\frac{\rho^2}{t'^2} + \frac{z^2}{t^2}}\right)}{\rho^2 + \frac{z^2 t'^2}{t^2}} \exp\left[-\frac{\left(\frac{\rho t}{zt'}\right)^2}{\Theta^2}\right] \exp\left[-\frac{t'}{\tau_0}\right] \quad (3.35)$$

Due to the singularity at  $t = 0$  in eqn. (2.35), we shall treat the lower limit as  $\tau = \frac{2\pi}{\Omega_{Ba}}$  instead of zero, where  $\Omega_{Ba}$  is the gyrofrequency of the barium ions, which has the numerical value of  $\tau = 0.180s^{-1}$ . Thus

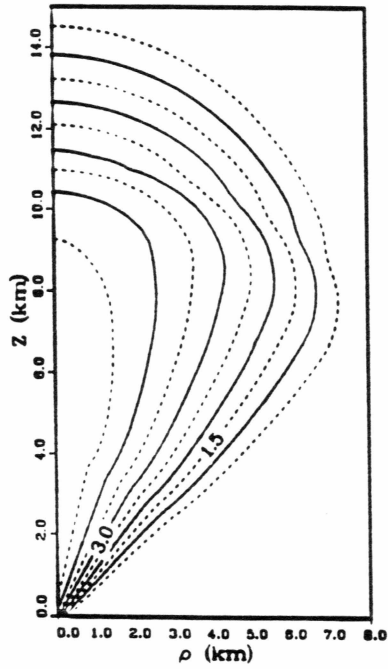
$$n_{Ba_0} = \frac{1}{\tau_0 t} \int_{\tau}^t dt' \frac{f\left(\sqrt{\frac{\rho^2}{t'^2} + \frac{z^2}{t^2}}\right)}{\rho^2 + \frac{z^2 t'^2}{t^2}} \exp\left[-\frac{\left(\frac{\rho t}{zt'}\right)^2}{\Theta^2}\right] \exp\left[-\frac{t'}{\tau_0}\right] \quad (3.36)$$

### 2.3 Calculations and Results of Number Densities

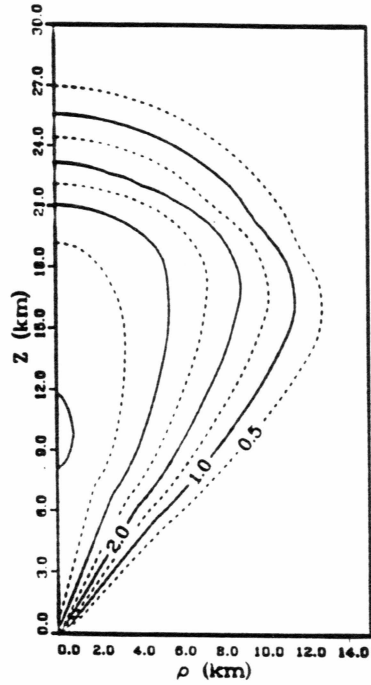
In the calculations for the number densities we set the angular width,  $\Theta$ , to be  $15^\circ$  and the photoionization rate,  $\tau_0$ , to be 20 sec [Drapatz, 1972]. Fig.1 shows the differential velocity distribution taken from Stenbaek-Nielsen et al., 1984.

Fig.2 shows contours of the logarithm of the neutral number densities for the times of 1, 2, 5, and 10 seconds. The plots have the z-axis parallel to the magnetic field. Fig.3 shows contours of the barium ion number densities at the same times and presented in the same manner. The distance scales in Fig.2 and Fig.3 are different for the various times. The distribution of the ions are greatly elongated in the z-direction. Note the difference in the  $\rho$ -scale and z-scale. Also, the plots at five and ten seconds show that the ion number density is greater than that of the neutrals within a kilometer of the z-axis.

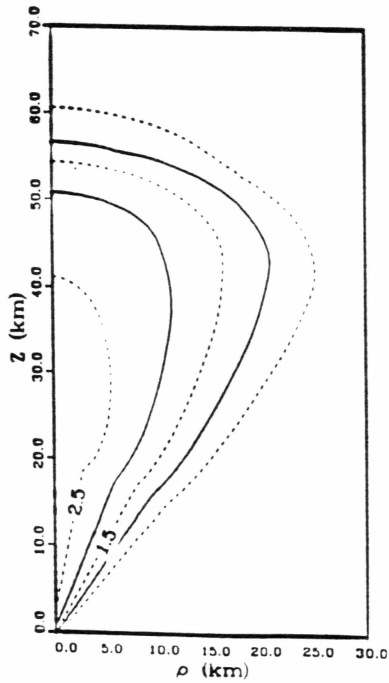
CONTOURS NEUTRAL BARIUM NO. DENSITY  
LOG 10 contours incremented by .5  
time= 1 sec



CONTOURS NEUTRAL BARIUM NO. DENSITY  
LOG 10 contours incremented by .5  
time= 2 sec



CONTOURS NEUTRAL BARIUM NO. DENSITY  
LOG 10 contours incremented by .5  
time= 5 sec



CONTOURS NEUTRAL BARIUM NO. DENSITY  
LOG 10 contours incremented by .5  
time= 10 sec

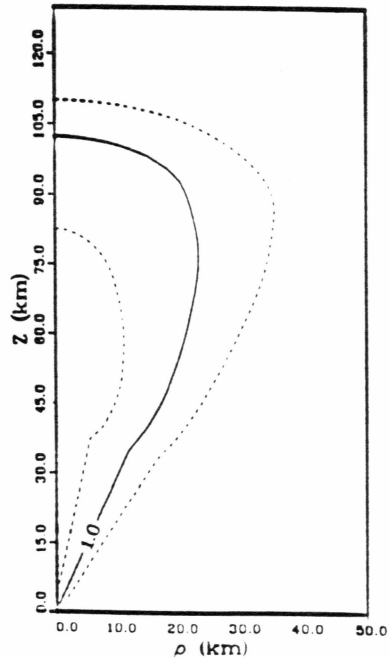
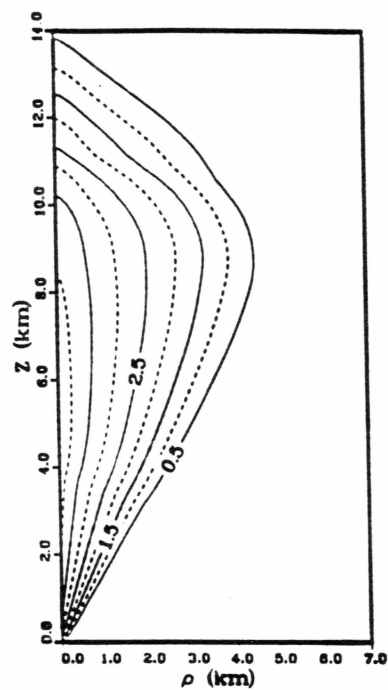
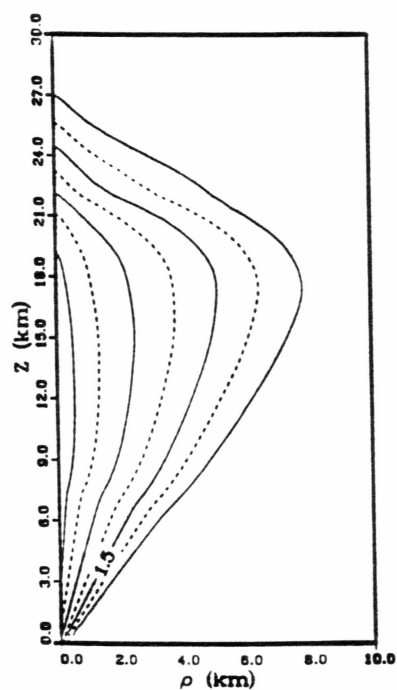


Figure 2: Number density contours of the barium atoms at times 1, 2, 5, and 10 seconds after detonation. The ejection is directed parallel to the magnetic field.

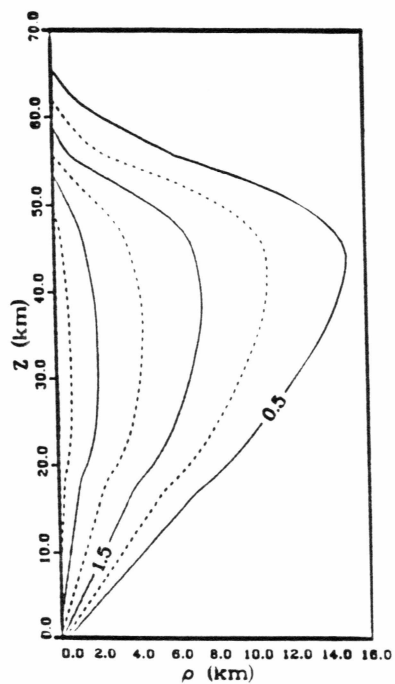
CONTOUR PLOT BARIUM ION NO. DENSITY  
LOG 10 contours incremented by .5  
time=1 sec



CONTOUR PLOT BARIUM ION NO. DENSITY  
LOG 10 contours incremented by .5  
time=2 sec



CONTOUR PLOT BARIUM ION NO. DENSITY  
LOG 10 contours incremented by .5  
time=5 sec



CONTOUR PLOT BARIUM ION NO. DENSITY  
LOG 10 contours incremented by .5  
time=10 sec

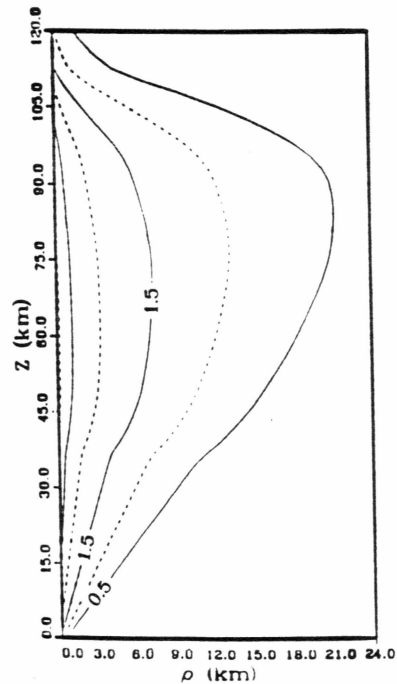


Figure 3: Number density contours of the barium ions at the same conditions as in Fig.2.

### Chapter 3: Derivation of the Dispersion Relation

In the following discussion we will derive the electrostatic dispersion relation that will be used to analyze instabilities that arise from the injection of barium ions in the ionosphere.

The behavior of the barium plasma can be described by the equation

$$\frac{\partial f_{Ba}(\mathbf{x}, \mathbf{v}, t)}{\partial t} + \mathbf{v} \cdot \nabla_{\mathbf{x}} f_{Ba} + \frac{q_{Ba}}{m_{Ba}} \left( \mathbf{E} + \frac{\mathbf{v}}{c} \times \mathbf{B} \right) \cdot \nabla_{\mathbf{v}} f_{Ba} = \frac{1}{\tau_o} n_n \delta^3 \left( \mathbf{v} - \frac{\mathbf{x}}{t} \right) \quad (3.1)$$

where  $f_{Ba}(\mathbf{x}, \mathbf{v}, t)$  is the distribution function associated with the barium ions. Eqn(3.1) states that the total time derivative of  $f_{Ba}$  along a particle orbit is equal to the decay of the neutrals present in a given volume element.

Since we're dealing with electrostatic waves the only Maxwell equation needed is Poisson's equation

$$\nabla \cdot \mathbf{E} = 4\pi\rho \quad (3.2)$$

In solving the equation above we partition the distribution function

$$f_{Ba} = f_{Ba_0} + f_{Ba_1} \quad (3.3)$$

into a zero order solution,  $f_{Ba_0}$ , and a small perturbation,  $f_{Ba_1}$ , associated with small amplitude waves.

We have assumed that there is a background magnetic field but no background electric field present. Thus, with the electrostatic approximations we have only a zero order magnetic field

$$\mathbf{B} = \mathbf{B}_0 \quad (3.4)$$

and a perturbed first order electric field

$$\mathbf{E} = \mathbf{E}_1 \quad (3.5)$$

The electrostatic approximation is justified due to the  $\beta$ , the ratio of the plasma pressure to the magnetic pressure, in the  $F_2$  region having the order of  $10^{-5}$ , which is much smaller than  $10^{-2}$  where electromagnetic effects become important [Hasegawa, 1975]. Also, since the effects of gravity are small compared to the electro-magnetic interactions we have not included gravity in this model.

Substituting equations (3.3), (3.4), and (3.5) into (3.1) and collecting the zero order terms we get the equation that describes the motion of the zero order particles.

$$\frac{\partial f_{Ba_0}}{\partial t} + \mathbf{v} \cdot \frac{\partial f_{Ba_0}}{\partial \mathbf{x}} + (\mathbf{v} \times \boldsymbol{\Omega}) \cdot \frac{\partial f_{Ba_0}}{\partial \mathbf{v}} = \frac{1}{\tau} n_n(z, \rho, t) \delta^3 \left( \mathbf{v} - \frac{\mathbf{x}}{t} \right) \quad (3.6)$$

which is the same as eqn. (2.13). It was shown in Chapter 2 that  $f_{Ba_0}$  was described by eqn(2.88). With the substitution of eqn(2.31) and eqn(2.32) into eqn(2.88) we can write the zero order distribution as

$$f_{Ba_0} = \frac{1}{2\pi\tau_0} \int_0^t dt' n_n(z', \rho, t') \delta \left( \frac{1}{t'} (v_{\parallel} t - z) \right) \frac{1}{v_{\perp}} \delta \left( v_{\perp} - \frac{\rho}{t'} \right) \quad (3.7)$$

We now proceed to do the integration with respect to  $t'$ . Using the identity [Jackson, 1975]

$$\delta(f(\mathbf{x})) = \sum_i \frac{1}{\left| \frac{df}{dx}(\mathbf{x}_i) \right|} \delta(\mathbf{x} - \mathbf{x}_i) \quad (3.8)$$

where  $f(\mathbf{x})$  has only simple zeros located at  $\mathbf{x}_i$ , eqn. (2.32) can be written as

$$\delta \left( v_{\perp} - \frac{\rho}{t'} \right) = \frac{1}{\frac{\rho}{t'^2}} \delta(t' - t_0) \quad (3.9)$$

where  $t_0 = \frac{\rho}{v_{\perp}}$ . Integrating this over  $t'$  we have

$$\int_0^t dt' \delta \left( v_{\perp} - \frac{\rho}{t'} \right) = \begin{cases} \frac{\rho}{v_{\perp}^2} & \frac{\rho}{v_{\perp}} < t \\ 0 & \frac{\rho}{v_{\perp}} > t \end{cases} \quad (3.10)$$

from eqn(2.29) we have

$$z' = z - v_{\parallel} \left( t - \frac{\rho}{v_{\perp}} \right)$$

Since there is a delta function on  $v_{\parallel} = \frac{z}{t}$

$$z' = z - \frac{z}{t} \left( 1 - \frac{\rho}{v_{\perp}} \right) = \frac{z\rho}{v_{\perp}t}$$

and the zero order distribution function takes the form

$$\begin{aligned} f_{Ba_0} &= \frac{1}{2\pi\tau_0} n_n \left( \frac{z\rho}{v_{\perp}t}, \rho, \frac{\rho}{v_{\perp}} \right) \frac{\rho}{v_{\perp}^3} \delta \left( \frac{v_{\perp}}{\rho} (v_{\parallel}t - z) \right) \\ &= \frac{1}{2\pi\tau_0} n_n \left( \frac{z\rho}{v_{\perp}t}, \rho, \frac{\rho}{v_{\perp}} \right) \frac{\rho^2}{v_{\perp}^4 t} \delta \left( v_{\parallel} - \frac{z}{t} \right) \end{aligned} \quad (3.11)$$

We have plotted  $f_{Ba_0}$  with respect to velocity in Fig.4, where  $t = 1s$ ,  $\rho = 1km$ , and  $z = 5km$ . This distribution function describes the perpendicular velocity distribution of the ions at a particular point in space and time. We note that the distribution function resembles a delta function plus a slight spread in velocity space.

With an expression for  $f_{Ba_0}$  we continue our derivation by solving for  $f_{Ba_1}$ . The first order terms upon substitution of eqn.(3.4) and eqn.(3.5) into (3.1) give the equation

$$\frac{\partial f_{Ba_1}}{\partial t} + \mathbf{v} \cdot \nabla_x f_{Ba_1} + \frac{q_{Ba}}{m_{Ba}} \mathbf{E}_1 \cdot \nabla_v f_{Ba_0} + \frac{q_{Ba}}{m_{Ba}} \left( \frac{\mathbf{v}}{c} \times \mathbf{B}_0 \right) \cdot \nabla_v f_{Ba_1} = 0 \quad (3.12)$$

because we assume an electrostatic perturbation,  $\nabla \times \mathbf{E} = 0$ , the electric potential can be used to represent the electric field

$$\mathbf{E}_1 = -\nabla_x \varphi \quad (3.13)$$

With this substitution the first order equation is

$$\frac{\partial f_{Ba_1}}{\partial t} + \mathbf{v} \cdot \frac{\partial f_{Ba_1}}{\partial \mathbf{x}} + (\mathbf{v} \times \boldsymbol{\Omega}_{Ba}) \cdot \frac{\partial f_{Ba_1}}{\partial \mathbf{v}} = \frac{q_{Ba}}{m_{Ba}} \frac{\partial \varphi}{\partial \mathbf{x}} \cdot \frac{\partial f_{Ba_0}}{\partial \mathbf{v}} \quad (3.14)$$

BARIUM ION DISTRIBUTION  
TIME=1 SEC  $z=5.0e5$  (cm)  $\rho=1.0e5$  (cm)

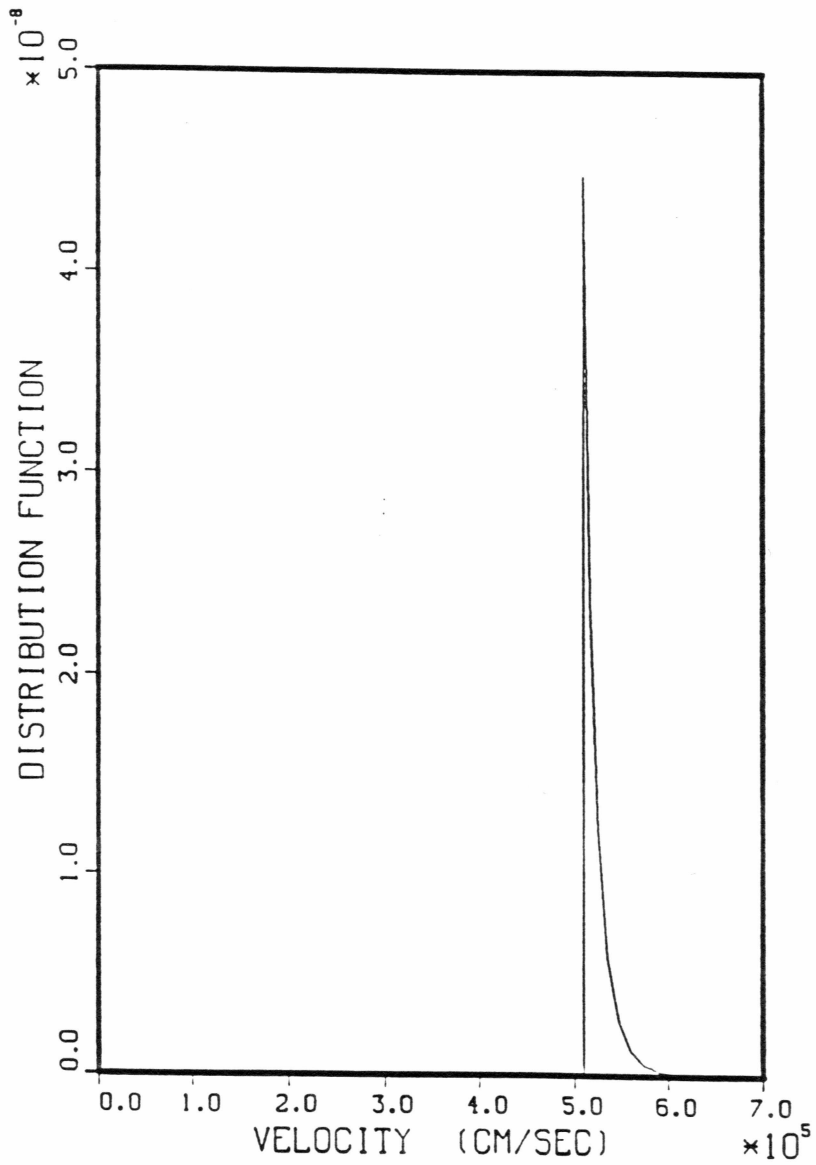


Figure 4: Distribution of barium ions associated with velocity for a position of  $z = 5km$ ,  $\rho = 1km$ , and a time of 1 second after detonation.



where  $\Omega_{Ba}$  is the cyclotron frequency of the barium ions in the direction of the magnetic field. The left side of eqn. (3.14) is a total derivative along helical orbits and can be written as

$$\frac{df_{Ba_1}}{dt} = \frac{q_{Ba}}{m_{Ba}} \frac{\partial \varphi}{\partial \mathbf{x}} \cdot \frac{\partial f_{Ba_0}}{\partial \mathbf{v}} \quad (3.15)$$

We can solve for  $f_{Ba_1}$  by integrating along the trajectories that satisfy the equation  $\ddot{\mathbf{x}} = \mathbf{v} \times \Omega_{Ba}$ , thus

$$f_{Ba_1} = \int_{-\infty}^t dt' \frac{q_{Ba}}{m_{Ba}} \frac{\partial \varphi}{\partial \mathbf{x}} \cdot \frac{\partial f_{Ba_0}}{\partial \mathbf{v}} \Big|_{v=v'(t')} \quad (3.16)$$

In choosing the magnetic field to be along the  $z$  axis the paths of the ions are described by [Hasegawa, 1975]

$$\begin{aligned} x'(t') - x &= \frac{v_{\perp}}{\Omega_{Ba}} \{ \sin [\Omega_{Ba}(t' - t) + \psi] - \sin \psi \} \\ y'(t') - y &= \frac{v_{\perp}}{\Omega_{Ba}} \{ \cos [\Omega_{Ba}(t' - t) + \psi] - \cos \psi \} \\ z'(t') - z &= v_{\parallel} (t' - t) \end{aligned} \quad (3.17)$$

and

$$\begin{aligned} v'_x(t') &= v_{\perp} \cos [\Omega_{Ba}(t' - t) + \psi] \\ v'_y(t') &= v_{\perp} \sin [\Omega_{ba}(t' - t) + \psi] \\ v'_z(t') &= v_{\parallel} \end{aligned} \quad (3.18)$$

the final position at  $t' = t$  is chosen to be  $x' = x$ ,  $y' = y$ , and  $z' = z$  while the corresponding velocities are  $v_x(t) = v_{\perp} \cos \psi$ ,  $v_y(t) = -v_{\perp} \sin \psi$ , and  $v_z(t) = v_{\parallel}$ . The sense of rotation is left-handed for the ions with respect to the magnetic field.

Now consider a perturbation of the form  $\exp [i(\mathbf{k} \cdot \mathbf{x} - \omega t)]$ , take the direction of propagation of the wave to be in the  $x, z$  plane such that

$$\mathbf{k} \cdot \mathbf{x} = k_{\perp} x + k_{\parallel} z \quad (3.19)$$

$$\varphi = \tilde{\varphi} \exp [i(k_{\parallel} z' + k_{\perp} x' - \omega t)] \quad (3.20)$$

and

$$\nabla_x \varphi(t') = i\mathbf{k}\varphi(t') \quad (3.21)$$

this gives the equation

$$f_{Ba_1}(x, v, t) = i \frac{q_{Ba}}{m_{Ba}} \tilde{\varphi} \int_{-\infty}^t dt' \left( k_{\parallel} \frac{\partial f_{Ba_0}}{\partial v_{\parallel}} + k_{\perp} \frac{\partial f_{Ba_0}}{\partial v_x} \right) \Big|_{v=v'(t')} \exp [i(k_{\parallel} z' + k_{\perp} x' - \omega t)] \quad (3.22)$$

since

$$v_{\perp} = \sqrt{v_x^2 + v_y^2}$$

then

$$\frac{\partial v_{\perp}}{\partial v_x} \Big|_{v=v'(t')} = \frac{v_x}{v_{\perp}} = \cos [\Omega_{Ba}(t' - t) + \psi] \quad (3.23)$$

Substituting eqn. (3.17) and eqn. (3.23) into eqn. (3.22) yields

$$f_{Ba_1} = i \frac{q_{Ba}}{m_{Ba}} \tilde{\varphi} \exp [i(\mathbf{k} \cdot \mathbf{x})] \int_{-\infty}^t dt' \left[ k_{\parallel} \frac{\partial f_{Ba_0}}{\partial v_{\parallel}} + k_{\perp} \frac{\partial f_{Ba_0}}{\partial v_{\perp}} \cos [\Omega_{Ba}(t' - t) + \psi] \right] \exp \left\{ i \left( k_{\parallel} v_{\parallel}(t' - t) + \frac{k_{\perp} v_{\perp}}{\Omega_{Ba}} \sin [\Omega_{Ba}(t' - t) + \psi] - \frac{k_{\perp} v_{\perp}}{\Omega_{Ba}} \sin \psi - \omega t' \right) \right\} \quad (3.24)$$

where  $v_{\parallel}$  and  $v_{\perp}$  are constants of motion. Using the identity [Hasegawa,1975]

$$\exp (iz \sin \psi) = \sum_{n=-\infty}^{\infty} J_n(z) \exp (in\psi) \quad (3.25)$$

we can write  $f_{Ba_1}$  as

$$\begin{aligned}
f_{Ba_1} = & i \frac{q_{Ba}}{m_{Ba}} \bar{\varphi} \exp [i(\mathbf{k} \cdot \mathbf{x} - \omega t)] \int_{-\infty}^t dt' \left\{ k_{\parallel} \frac{\partial f_{Ba_0}}{\partial v_{\parallel}} + k_{\perp} \frac{\partial f_{Ba_0}}{\partial v_{\perp}} \right. \\
& \left. \frac{1}{2} \left( \exp [i(\Omega_{Ba}(t' - t) + \psi)] + \exp [-i(\Omega_{Ba}(t' - t) + \psi)] \right) \right\} \\
& \sum_{n=-\infty}^{\infty} \sum_{l=-\infty}^{\infty} J_n \left( \frac{k_{\perp} v_{\perp}}{\Omega_{Ba}} \right) J_l \left( \frac{k_{\perp} v_{\perp}}{\Omega_{Ba}} \right) \exp [i(k_{\parallel} v_{\parallel} + n\Omega_{Ba} - \omega)(t' - t)] \\
& \exp [i(n - l)\psi]
\end{aligned} \tag{2.26}$$

Since we are interested in plasma instabilities, where the imaginary part of  $\omega$  is positive, we can evaluate the integral over  $t'$  by using the fact that  $\frac{\partial f}{\partial v_{\parallel}}$  and  $\frac{\partial f}{\partial v_{\perp}}$  are independent of time and shifting the indices of the Bessel functions up and down by one [Xin, 1987].

$$\begin{aligned}
f_{Ba_1} = & \frac{q_{Ba}}{m_{Ba}} \varphi(t) \sum_{n=-\infty}^{\infty} \sum_{l=-\infty}^{\infty} J_l \left( \frac{k_{\perp} v_{\perp}}{\Omega_{Ba}} \right) \frac{\exp [i(n - l)\psi]}{[k_{\parallel} v_{\parallel} + n\Omega_{Ba} - \omega]} \\
& \left\{ k_{\perp} \frac{\partial f_{Ba_0}}{\partial v_{\parallel}} J_n \left( \frac{k_{\perp} v_{\perp}}{\Omega_{Ba}} \right) + \frac{k_{\perp}}{2} \frac{\partial f_{Ba_0}}{\partial v_{\perp}} \left[ J_{n-1} \left( \frac{k_{\perp} v_{\perp}}{\Omega_{Ba}} \right) + J_{n+1} \left( \frac{k_{\perp} v_{\perp}}{\Omega_{Ba}} \right) \right] \right\}
\end{aligned} \tag{3.27}$$

Finally, with the use of the identity

$$J_{n-1}(z) + J_{n+1}(z) = \frac{2n}{z} J_n(z) \tag{3.28}$$

the first order distribution function is described by

$$\begin{aligned}
f_{Ba_1} = & \frac{q_{Ba}}{m_{Ba}} \varphi(t) \sum_{n=-\infty}^{\infty} \sum_{l=-\infty}^{\infty} J_n \left( \frac{k_{\perp} v_{\perp}}{\Omega_{Ba}} \right) J_l \left( \frac{k_{\perp} v_{\perp}}{\Omega_{Ba}} \right) \\
& \left[ \frac{k_{\parallel} \frac{\partial f_{Ba_0}}{\partial v_{\parallel}} + \frac{n\Omega_{Ba}}{v_{\perp}} \frac{\partial f_{Ba_0}}{\partial v_{\perp}}}{k_{\parallel} v_{\parallel} + n\Omega_{Ba} - \omega} \right] \exp [i(n - l)\psi]
\end{aligned} \tag{3.29}$$

The first order barium ion number density,  $n_{Ba_1}$ , is calculated by the integration of  $f_{Ba_1}$  over velocity space

$$n_{Ba_1} = \int d^3 v f_{Ba_1} \tag{3.30}$$

where

$$d^3v = dv_{\parallel} dv_{\perp} dv_{\perp}$$

thus

$$n_{Ba_1} = \frac{q_{Ba}}{m_{Ba}} \varphi(t) \int_0^{2\pi} d\psi \int_0^{\infty} dv_{\parallel} \int_{\frac{\ell}{4}}^{\infty} v_{\perp} dv_{\perp} \sum_{n=-\infty}^{\infty} \sum_{l=-\infty}^{\infty} J_n \left( \frac{k_{\perp} v_{\perp}}{\Omega_{Ba}} \right) J_l \left( \frac{k_{\perp} v_{\perp}}{\Omega_{Ba}} \right) \frac{k_{\parallel} \frac{\partial f_{Ba_0}}{\partial v_{\parallel}} + \frac{n\Omega_{Ba}}{v_{\perp}} \frac{\partial f_{Ba_0}}{\partial v_{\perp}}}{k_{\parallel} v_{\parallel} + n\Omega_{Ba} - \omega} \exp[i(n-l)\psi] \quad (3.31)$$

Since

$$\int_0^{2\pi} d\psi \exp[i(n-l)\psi] = 2\pi \delta_{nl} \quad (3.32)$$

the integration over  $\psi$  yields [Hasegawa,1975]

$$n_{Ba_1} = \frac{2\pi q_{Ba}}{m_{Ba}} \varphi(t) \sum_{n=-\infty}^{\infty} \int_0^{\infty} dv_{\parallel} \int_{\frac{\ell}{4}}^{\infty} v_{\perp} dv_{\perp} J_n^2 \left( \frac{k_{\perp} v_{\perp}}{\Omega_{Ba}} \right) \frac{k_{\perp} \frac{\partial f_{Ba_0}}{\partial v_{\parallel}} + \frac{n\Omega_{Ba}}{v_{\perp}} \frac{\partial f_{Ba_0}}{\partial v_{\perp}}}{k_{\parallel} v_{\parallel} + n\Omega_{Ba} - \omega} \quad (3.33).$$

In proceeding with the derivation of  $n_{Ba_1}$  we split up the integration into two terms

such that

$$n_{Ba_1} = \frac{q_{Ba}}{m_{Ba}} \varphi(t) \sum_{n=-\infty}^{\infty} (T_{n_{\parallel}} + T_{n_{\perp}}) \quad (3.34)$$

where

$$T_{n_{\parallel}} = 2\pi \int_0^{\infty} dv_{\parallel} \int_{\frac{\ell}{4}}^{\infty} v_{\perp} dv_{\perp} J_n^2 \left( \frac{k_{\perp} v_{\perp}}{\Omega_{Ba}} \right) \frac{k_{\parallel} \frac{\partial f_{Ba_0}}{\partial v_{\parallel}}}{k_{\parallel} v_{\parallel} + n\Omega_{Ba} - \omega} \quad (3.35)$$

and

$$T_{n_{\perp}} = 2\pi \int_0^{\infty} dv_{\parallel} \int_{\frac{\ell}{4}}^{\infty} v_{\perp} dv_{\perp} J_n^2 \left( \frac{k_{\perp} v_{\perp}}{\Omega_{Ba}} \right) \frac{\frac{n\Omega_{Ba}}{v_{\perp}} \frac{\partial f_{Ba_0}}{\partial v_{\perp}}}{k_{\parallel} v_{\parallel} + n\Omega_{Ba} - \omega} \quad (3.36)$$

In order to avoid integrating over the derivatives of the discontinuous distribution functions, we integrate by parts and cast the partial derivatives onto other portions of the integrand.

$$T_{n_{\parallel}} = 2\pi \int_{\frac{\ell}{4}}^{\infty} v_{\perp} dv_{\perp} J_n^2 \left( \frac{k_{\perp} v_{\perp}}{\Omega_{Ba}} \right) \int_0^{\infty} dv_{\parallel} \frac{f_{Ba_0}}{\left[ v_{\parallel} - \left( \frac{\omega - n\Omega_{Ba}}{k_{\parallel}} \right) \right]^2} \quad (3.37)$$

and

$$T_{n_{\perp}} = \frac{-2\pi n \Omega_{Ba}}{k_{\parallel}} \int_{\frac{\rho}{t}}^{\infty} dv_{\perp} \frac{\partial}{\partial v_{\perp}} \left[ J_n^2 \left( \frac{k_{\perp} v_{\perp}}{\Omega_{Ba}} \right) \right] \int_0^{\infty} dv_{\parallel} \frac{f_{Ba_0}}{\left[ v_{\parallel} - \left( \frac{\omega - n \Omega_{Ba}}{k_{\parallel}} \right) \right]} \quad (3.38)$$

Substituting  $f_{Ba_0}$  into  $T_{n_{\parallel}}$  and  $T_{n_{\perp}}$  yields

$$T_{n_{\parallel}} = 2\pi \int_{\frac{\rho}{t}}^{\infty} v_{\perp} dv_{\perp} J_n^2 \left( \frac{k_{\perp} v_{\perp}}{\Omega_{Ba}} \right) \int_0^{\infty} dv_{\parallel} \frac{\frac{1}{2\pi\tau_0} n_n \left( \frac{z\rho}{v_{\perp}t}, \rho, \frac{\rho}{t} \right) \frac{\rho^2}{v_{\perp}^4 t} \delta \left( v_{\parallel} - \frac{z}{t} \right)}{\left[ v_{\parallel} - \left( \frac{\omega - n \Omega_{Ba}}{k_{\parallel}} \right) \right]^2} \quad (3.39)$$

$$T_{n_{\perp}} = -\frac{2\pi n \Omega_{Ba}}{k_{\parallel}} \int_{\frac{\rho}{t}}^{\infty} dv_{\perp} \frac{\partial}{\partial v_{\perp}} \left[ J_n^2 \left( \frac{k_{\perp} v_{\perp}}{\Omega_{Ba}} \right) \right] \int_0^{\infty} dv_{\parallel} \frac{\frac{1}{2\pi\tau_0} n_n \left( \frac{z\rho}{v_{\perp}t}, \rho, \frac{\rho}{v_{\perp}} \right) \frac{\rho^2}{v_{\perp}^4 t} \delta \left( v_{\parallel} - \frac{z}{t} \right)}{\left[ v_{\parallel} - \left( \frac{\omega - n \Omega_{Ba}}{k_{\parallel}} \right) \right]} \quad (3.40)$$

Doing the integration with respect to the parallel velocity we obtain

$$T_{n_{\parallel}} = \frac{1}{\tau_0} \frac{1}{\left[ \frac{z}{t} - \left( \frac{\omega - n \Omega_{Ba}}{k_{\parallel}} \right) \right]^2} \int_{\frac{\rho}{t}}^{\infty} dv_{\perp} J_n^2 \left( \frac{k_{\perp} v_{\perp}}{\Omega_{Ba}} \right) n_n \left( \frac{z\rho}{v_{\perp}t}, \rho, \frac{\rho}{v_{\perp}} \right) \frac{\rho^2}{v_{\perp}^3 t} \quad (3.41)$$

$$T_{n_{\perp}} = -\frac{n \Omega_{Ba}}{k_{\parallel} \tau_0} \frac{1}{\left[ \frac{z}{t} - \left( \frac{\omega - n \Omega_{Ba}}{k_{\parallel}} \right) \right]} \int_{\frac{\rho}{t}}^{\infty} dv_{\perp} \left[ \frac{\partial}{\partial v_{\perp}} J_n^2 \left( \frac{k_{\perp} v_{\perp}}{\Omega_{Ba}} \right) \right] n_n \left( \frac{z\rho}{v_{\perp}t}, \rho, \frac{\rho}{v_{\perp}} \right) \frac{\rho^2}{v_{\perp}^4 t} \quad (3.42)$$

Now to simplify the form of  $T_{n_{\perp}}$  we note that

$$\frac{\partial}{\partial v_{\perp}} J_n^2 \left( \frac{k_{\perp} v_{\perp}}{\Omega_{Ba}} \right) = \frac{2k_{\perp}}{\Omega_{Ba}} J_n' \left( \frac{k_{\perp} v_{\perp}}{\Omega_{Ba}} \right) J_n \left( \frac{k_{\perp} v_{\perp}}{\Omega_{Ba}} \right) \quad (3.43)$$

and by using the identity

$$J_n'(z) = \frac{1}{2} [J_{n-1}(z) - J_{n+1}(z)] \quad (3.44)$$

we get

$$T_{n_{\perp}} = -\frac{n \Omega_{Ba}}{k_{\parallel} \tau_0} \frac{1}{\left[ \frac{z}{t} - \left( \frac{\omega - n \Omega_{Ba}}{k_{\parallel}} \right) \right]} \int_{\frac{\rho}{t}}^{\infty} dv_{\perp} \frac{k_{\perp}}{\Omega_{Ba}} J_n \left( \frac{k_{\perp} v_{\perp}}{\Omega_{Ba}} \right) \left[ J_{n-1} \left( \frac{k_{\perp} v_{\perp}}{\Omega_{Ba}} \right) - J_{n+1} \left( \frac{k_{\perp} v_{\perp}}{\Omega_{Ba}} \right) \right] \frac{\rho^2}{v_{\perp}^4 t} n_n \left( \frac{z\rho}{v_{\perp}t}, \rho, \frac{\rho}{v_{\perp}} \right) \quad (3.45)$$

Finally for the first order barium number distribution we have

$$n_{Ba_1} = \frac{q_{Ba}}{m_{Ba}} \varphi(t) [T_{n_{\parallel}} + T_{n_{\perp}}] \quad (3.34)$$

where

$$T_{n_{\parallel}} = \frac{1}{\tau_o} \frac{1}{\left[ \frac{z}{t} - \left( \frac{\omega - n\Omega_{Ba}}{k_{\parallel}} \right) \right]^2} \int_{\frac{z}{t}}^{\infty} dv_{\perp} J_n^2 \left( \frac{k_{\perp} v_{\perp}}{\Omega_{Ba}} \right) \frac{\rho^2}{v_{\perp}^3 t} n_n \left( \frac{z\rho}{v_{\perp} t}, \rho, \frac{\rho}{v_{\perp}} \right) \quad (3.41)$$

$$T_{n_{\perp}} = -\frac{nk_{\perp}}{k_{\parallel} \tau_o} \frac{1}{\left[ \frac{z}{t} - \left( \frac{\omega - n\Omega_{Ba}}{k_{\parallel}} \right) \right]} \int_{\frac{z}{t}}^{\infty} dv_{\perp} J_n \left( \frac{k_{\perp} v_{\perp}}{\Omega_{Ba}} \right) \left[ J_{n-1} \left( \frac{k_{\perp} v_{\perp}}{\Omega_{Ba}} \right) - J_{n+1} \left( \frac{k_{\perp} v_{\perp}}{\Omega_{Ba}} \right) \right] \frac{\rho^2}{v_{\perp}^4 t} n_n \left( \frac{z\rho}{v_{\perp} t}, \rho, \frac{\rho}{v_{\perp}} \right) \quad (3.46)$$

and where

$$n_n \left( \frac{z\rho}{v_{\perp} t}, \rho, \frac{\rho}{v_{\perp}} \right) = \frac{v_{\perp}}{\rho^3 \left( 1 + \frac{z^2}{v_{\perp}^2 t^2} \right)} f \left( \sqrt{v_{\perp}^2 + \frac{z^2}{t^2}} \right) \exp \left[ -\frac{(v_{\perp} z/t)^2}{\Theta^2} \right] \exp \left[ -\frac{\rho}{v_{\perp} \tau_o} \right] \quad (3.47)$$

The integrals for  $T_{n_{\parallel}}$  and  $T_{n_{\perp}}$  must be calculated numerically since it is not possible to integrate them analytically.

Now we consider the background plasma of electrons and oxygen ions. The zero order distribution function for the background plasmas are assumed to be Maxwellian distributions

$$f_{s_0} = n_{s_0} \left( \frac{1}{\sqrt{\pi} v_{th_s}} \right)^3 \exp \left[ -\frac{v^2}{v_{th_s}^2} \right] \quad (3.48)$$

where  $v_{th_s} = \sqrt{\frac{2T_s}{m_s}}$  is the thermal velocity and  $T_s$  involves the boltzmann constant. Substituting eqn. (3.48) into eqn. (3.33) we get [Xin, 1987]

$$n_{s_1} = \int_0^{2\pi} d\psi \int_{-\infty}^{\infty} dv_{\parallel} \int_0^{\infty} v_{\perp} dv_{\perp} f_{s_1}$$

$$n_{s_1} = n_{s_0} \frac{q_s}{m_s} \varphi \frac{-2}{v_t h_s} \left( \frac{1}{\sqrt{\pi} v_t h_s} \right)^3 \sum_{n=-\infty}^{\infty} \sum_{l=-\infty}^{\infty} 2\pi \delta_{nl}$$

$$\begin{aligned}
& \int_{-\infty}^{\infty} dv_{\parallel} \frac{k_{\parallel} v_{\parallel} + n\Omega_s}{k_{\parallel} v_{\parallel} + n\Omega_s - \omega} \exp \left[ -\frac{v_{\parallel}^2}{v_{th_s}^2} \right] \\
& \int_0^{\infty} v_{\perp} dv_{\perp} J_n \left( \frac{k_{\perp} v_{\perp}}{\Omega_s} \right) J_l \left( \frac{k_{\perp} v_{\perp}}{\Omega_s} \right) \exp \left[ -\frac{v_{\perp}^2}{v_{th_s}^2} \right] \\
n_{s_1} &= 2\pi n_{s_0} \frac{q_s}{m_s} \varphi \frac{-2}{v_{th_s}^2} \left( \frac{1}{\sqrt{\pi} v_{th_s}} \right)^3 \sum_{n=-\infty}^{\infty} \\
& \int_{-\infty}^{\infty} dv_{\parallel} \frac{k_{\parallel} v_{\parallel} + n\Omega_s}{k_{\parallel} v_{\parallel} + n\Omega_s - \omega} \exp \left[ -\frac{v_{\parallel}^2}{v_{th_s}^2} \right] \\
& \int_0^{\infty} v_{\perp} dv_{\perp} J_n^2 \left( \frac{k_{\perp} v_{\perp}}{\Omega_s} \right) \exp \left[ -\frac{v_{\perp}^2}{v_{th_s}^2} \right]
\end{aligned} \tag{3.49}$$

The integral with respect to  $v_{\perp}$  can be evaluated as

$$\int_0^{\infty} v_{\perp} dv_{\perp} J_n^2 \left( \frac{k_{\perp} v_{\perp}}{\Omega_s} \right) \exp \left[ -\frac{v_{\perp}^2}{v_{th_s}^2} \right] = \frac{v_{th_s}^2}{2} I_n \left( \frac{k_{\perp}^2 v_{th_s}^2}{2\Omega_s^2} \right) \exp \left[ -\frac{k_{\perp}^2 v_{th_s}^2}{2\Omega_s^2} \right] \tag{3.50}$$

While the integral with respect to  $v_{\parallel}$  can be evaluated by making use of the plasma dispersion function which is [Hasegawa,1975]

$$Z(\zeta) = \frac{1}{\sqrt{\pi}} \int_{-\infty}^{\infty} \frac{\exp(-x^2)}{x - \zeta} dx \tag{3.51}$$

setting  $x = \frac{v_{\parallel}}{v_{th_s}}$  we obtain

$$\begin{aligned}
& \int_{-\infty}^{\infty} dv_{\parallel} \frac{k_{\parallel} v_{\parallel} + n\Omega_s}{k_{\parallel} v_{\parallel} + n\Omega_s - \omega} \exp \left[ -\frac{v_{\parallel}^2}{v_{th_s}^2} \right] \\
&= v_{th_s} \int_{-\infty}^{\infty} dx \left[ 1 + \frac{\frac{\omega}{k_{\parallel} v_{th_s}}}{x - \left( \frac{\omega - n\Omega_s}{k_{\parallel} v_{th_s}} \right)} \right] \exp(-x^2) \\
&= v_{th_s} \sqrt{\pi} \left[ 1 + \frac{\omega}{k_{\parallel} v_{th_s}} Z \left( \frac{\omega - n\Omega_s}{k_{\parallel} v_{th_s}} \right) \right]
\end{aligned} \tag{3.52}$$

Bringing these results together we have [Xin, 1987]

$$n_{s_1} = \frac{-2n_{s_0} q_s \varphi}{m_s v_{th_s}} \sum_{n=-\infty}^{\infty} I_n \left( \frac{k_{\perp}^2 v_{th_s}^2}{2\Omega_s^2} \right) \exp \left[ -\frac{k_{\perp}^2 v_{th_s}^2}{2\Omega_s^2} \right] \left[ 1 + \frac{\omega}{k_{\parallel} v_{th_s}} Z \left( \frac{\omega - n\Omega_s}{k_{\parallel} v_{th_s}} \right) \right] \tag{3.53}$$

Substituting  $\mathbf{E} = -\nabla\varphi$  into p's equation gives

$$-\nabla^2\varphi = 4\pi\rho \quad (3.54)$$

We assumed that at the start

$$n_{Ba_0} + n_{O_0} = n_{e_0}$$

thus eqn. (3.54) becomes

$$k^2\varphi = 4\pi e(n_{Ba_1} + n_{O_1} - n_{e_1}) \quad (3.55)$$

Upon substituting eqn. (3.34) and (3.53) into eqn. (3.55) and dividing by  $k^2\varphi$  we obtain

$$\begin{aligned} & 1 + \frac{1}{k^2\lambda_e^2} \left[ 1 + \sum_{n=-\infty}^{\infty} I_n(\mu_e) \exp[-\mu_e] \frac{\omega}{k_{\parallel}v_{th_e}} Z\left(\frac{\omega - n\Omega_e}{k_{\parallel}v_{th_e}}\right) \right] \\ & + \frac{1}{k^2\lambda_O^2} \left[ 1 + \sum_{n=-\infty}^{\infty} I_n(\mu_O) \exp[-\mu_O] \frac{\omega}{k_{\parallel}v_{th_O}} Z\left(\frac{\omega - n\Omega_O}{k_{\parallel}v_{th_O}}\right) \right] \\ & - \frac{4\pi e^2}{k^2 m_{Ba}} \sum_{n=-\infty}^{\infty} T_{n_{\parallel}} + T_{n_{\perp}} = 0 \end{aligned} \quad (3.56)$$

where

$$\begin{aligned} \lambda_s &= \left( \frac{8\pi n_{s_0} e^2}{m_s v_{th_s}^2} \right)^{-\frac{1}{2}} \\ \mu_s &= \left( \frac{k_{\perp}^2 v_{th_s}^2}{2\Omega_s^2} \right) \end{aligned}$$

and  $T_{n_{\parallel}}$  and  $T_{n_{\perp}}$  are described by eqn(3.41) and eqn(3.46), respectively. Also, we have made use of the identity

$$\sum_{n=-\infty}^{\infty} I_n(\mu_s) \exp[-\mu_s] = 1$$

The above equation, (3.56), is the dispersion relation that we shall analyze.



## Chapter 4: Calculation of the Dispersion Relation for a Particular Model

In this chapter we will choose parameters for the dispersion relation to model the barium ion injection into the ionosphere. The derived expression will be solved numerically to determine ion cyclotron growth rates for two cases. The first case does not assume an ambient oxygen ion background and the second does assume an ambient oxygen ion background.

### 4.1 Parameters

The shaped charge barium release experiments of [Wescott et al., 1975a], [Wescott et al., 1975b], and [Wescott et al., 1986a] have taken place in the upper  $F_2$  region, characteristically between 400 to 600 km. The experiments were oriented such that the injected barium would be directed nearly parallel to the magnetic field of the earth. Our model is for such a case.

It is known that the major ion constituent of the  $F_2$  region is monatomic oxygen ( $O^+$ ). Thus our model will consist of streaming barium ions with background distributions of monatomic oxygen and electrons [Banks and Kockarts, 1973].

In the ionospheric F region the number density of the oxygen ions varies with the time and altitude in the range of  $10^2$  to  $10^5$  per cubic centimeter. The oxygen ion temperature varies from  $1000K$  to  $2000K$  and the electron temperature is characteristically higher by a factor of two [Banks and Kockarts, 1973]. We have taken the monatomic oxygen temperature and number density to be

$$T_O = 1200K$$

$$n_{O_0} = 1000cm^{-3}$$

charge neutrality requires we set

$$n_{e_0} = n_{O_0} + n_{Ba_0}$$

The temperature for the electrons is

$$T_e = 2400K$$

The barium number density is determined from equation (2.36) in Chapter 2 by numerical integration. We take the magnetic field to be 0.5 gauss.

In a previous study Kindel and Kennel, [1971] showed that electrostatic waves could be excited by field-aligned currents. These waves could be electrostatic ion acoustic and ion cyclotron waves depending on the streaming velocity and the plasma temperature. In their paper they dealt with the case of electrons streaming along a magnetic field through a background of oxygen ions. It was shown that when the temperature ratio of the electrons to ions reached .02 to 20, the critical drift velocity for the electrostatic ion cyclotron instability was smaller than for the ion acoustic instability. They went on to point out that when a heavy ion is introduced into a light ion plasma it should increase the range of  $\frac{T_i}{T_e}$  for ion cyclotron wave dominance.

Xin, [1987] studied the case where barium ions were streaming along a magnetic field through a background plasma composed of electrons and ions. It was shown, that for conditions where the temperature ratio  $\frac{T_{Ba}}{T_e} = 0.5$ ,  $\frac{T_O}{T_e} = 1.0$ , and the ratio of the drift velocity to the thermal velocity of the barium ions  $u/v_{th_{Ba}} = 23.5$ , the first harmonic ion cyclotron wave was dominant and that the maximum growth rate occurred when the oxygen number density equaled the barium number density. Also, the growth rate was found to be sensitive to the electron temperature.

The cases studied by Xin, [1987] and Kindel and Kennel, [1971] assumed Maxwellian distributions drifting along a magnetic field to characterize the beam species. This gave each system an unstable distribution in velocity space parallel to the magnetic field. The present study differs from these in that the free energy that arises is due to the barium's motion perpendicular to the magnetic field, as shown in Fig.4. It should therefore be expected that the roots will differ some from the above studies.

Roots are now sought that satisfy the dispersion relation for the above described parameters.

Since this study is only interested with instabilities, roots are sought in which  $Im(\omega) > 0$ . This is due to the assumption that the wave behaves as  $\exp[\mathbf{k} \cdot \mathbf{x} - \omega t]$ . When the wave number  $\mathbf{k}$  has real values the frequency takes the form  $\omega = \omega_r + i\gamma$  and the exponential expression becomes  $\exp[i\mathbf{k} \cdot \mathbf{x} - i\omega t + \gamma t]$ .

In determining roots for the dispersion relation we must stay within the framework of our assumptions. Since the dispersion relation is dependent upon position and time after detonation we must choose these variables such that the time is long enough to average over the gyrofrequency and the position is far enough away from the magnetic field axis compared to the gyroradius. For these reasons a time of 1 second and a position of  $z = 5km$ ,  $\rho = 1km$  has been picked. Where the  $z$  represents the distance from the detonation site in the direction of the magnetic field and  $\rho$  the distance in the direction perpendicular to the field. This time and position corresponds to a barium ion number density of  $1618.cm^{-3}$ . Another reason we picked the above position was to be within the neutral beam half angle  $\Theta = 15^\circ$ .

## 4.2 No Ambient Plasma

The interest of this study is in looking for electrostatic ion cyclotron waves. In order to determine values of  $\mathbf{k}$  corresponding to growing waves, zero frequency instabilities perpendicular to the magnetic field are sought for a plasma consisting of barium ions and electrons only. These instabilities should be expected since our transverse velocity distribution somewhat resembles a delta function [Crawford and Tataronis, 1965].

The pure imaginary roots found had a maximum growth rate of  $\gamma = 22.09 \text{ s}^{-1}$  for a wave number of  $k = 1.98 \times 10^{-3} \text{ cm}^{-1}$ . These roots have a first peak at  $(\frac{k_{\perp} v_{\perp}}{\Omega_{Ba}}) \approx 2.25$  and subsequent peaks occur at intervals of  $\Delta(\frac{k_{\perp} v_{\perp}}{\Omega_{Ba}}) \approx \pi$ . In Fig.5 the growth rate divided by the barium ion cyclotron frequency  $(\frac{\gamma}{\Omega_{Ba+}})$  versus the perpendicular wave number multiplied by the gyroradius  $(\frac{k_{\perp} v_{\perp}}{\Omega_{Ba}})$  has been plotted. The second peak has the highest growth rate and as the wave number is increased further the peak growth rates diminish.

From the peak growth rates of the zero frequency instability waves are sought propagating a little off from the normal of the magnetic field. Using the wave number of the first peak  $k = 9.4 \times 10^{-4} \text{ cm}^{-1}$ , roots were then found for the angles between 89.9 and 89.995 degrees from the magnetic field and over a range of wave numbers.

Plotted in Figures 6a-7a and 6b-7b are the growth rates and frequencies associated with the first and second harmonics of the barium gyrofrequency  $\Omega_{Ba} = 35.12$  for the case where there is no oxygen ion background. The growth rates, Fig.6a-7a, have been plotted against the propagation angle  $\psi$  and the quantity  $\frac{k_{\perp} v_{\perp}}{\Omega_{Ba}}$ . The frequencies, Fig.6b-7b, have been plotted against the same arguments, but note that the axis for  $\psi$  has been reversed, in order to give a better view of the surface. Each curve in a plot represents a particular magnitude of  $\mathbf{k}$  and the graph on the back wall of each plot is the curve associated with the

largest growth rate for that plot. In Fig.6a the most striking feature is that there are two peaks in some of the curves for the finite growth rate as a function of  $\psi$ , while in others there is only one. This is a consequence of the way the terms for the electron and barium expressions in the dispersion equation in (3.56) behave. For the five curves that only have one peak, the first,  $n=1$ , term of the barium expression is dominant through the range of angles; this term is balanced by the electron term. In the curves with two peaks, the same is true except that as the frequency decreases closer to zero and the angle approaches  $90^\circ$  the electron term becomes small due to the parallel phase velocity being much greater than the electron thermal velocity. The first,  $n=1$ , barium term of eqn.(3.46) then interacts with the higher gyroharmonic terms of the barium expression  $T_{n\perp}$  of eqn.(3.46) to give the perpendicular propagating roots. The  $T_{n\parallel}$  expressions of eqn.(3.41) do not influence the roots for wave numbers with angles near  $90^\circ$ . The apparent discontinuity in the roots of Fig.6a is actually where the second harmonic roots, shown in Fig.7a-7b, take over. Fig.7a-7b shows the continuation of the features from Fig.6a-6b. The plot of the second harmonic shows the same pattern as the first harmonic but now the curves start with the second,  $n=2$ , barium term in the expansion of eqn.(3.46) dominating. For those curves that have the real part of the frequency decreasing to zero with a finite growth rate as the wave normal angle of propagation tends to  $90^\circ$ , the electron term of the dispersion equation becomes small. The second,  $n=2$ , barium term dominates at first then at the beginning of the next peak the first,  $n=1$ , term dominates. Finally, when the frequency approaches zero and the angle is nearly  $90^\circ$  we get the zero frequency instability of Crawford and Tataronis. The second harmonic term also has finite frequency perpendicular propagating roots. One of these roots is shown quite well in the curves on the back walls of figures 7a and 7b. These

curves start with the second,  $n=2$ , barium term dominating and it continues over the range of angles. The reason we obtain the finite frequency perpendicular instability is because the electron term becomes small as we approach  $90^\circ$  for this particular  $\mathbf{k}$ . The second,  $n=2$ , term in the expansion for the barium expression is then balanced by other terms in the barium expression. If we continue our examination for the third harmonic we would see a continuation of still higher growth rates. We find that our roots for perpendicular propagation indicate higher growth rates for larger wave numbers which agrees with the results of Crawford and Tataronis, [1965].

### 4.3 Effects of Ambient Plasma

In the figures 8a-11a the growth rates for the first four harmonics associated with the barium gyrofrequency for the case with an oxygen ion background have been plotted. These plots have similar labels for the axes as before but note that the  $\frac{k_{\perp} v_{\perp}}{\Omega_{Ba}}$  axis has been reversed to show a better view of the surface. Figures 8b-11b are the same as before but with the  $\frac{k_{\perp} v_{\perp}}{\Omega_{Ba}}$  axis reversed. The curves on the back walls are the curves associated with the largest growth rates and each curve still represents a particular magnitude of  $\mathbf{k}$ . Fig.8a shows that the maximum growth rate of the first gyroharmonic occurs for  $k = 8 \times 10^{-4}$  propagating at an angle of  $\psi = 89.97^\circ$ . The waves corresponding to the peak are being driven by the  $n=1$  barium term. We note that in comparing Fig.6a with Fig.8a that we have no zero frequency growing modes of the Crawford and Tataronis, [1965] type at  $90^\circ$  in Fig.8a. This is due to the effect of the ambient oxygen background. The  $n=0$  term of the oxygen expression is dominant and has little change over the range of angles plotted. The reason for this is that the main contribution to the oxygen term is from  $\frac{1}{k^2 \lambda_O^2} [1 - I_0(\mu_O) \exp(-\mu_O)]$ , where  $\mu_O$  and  $\lambda_O$  are described in eqn(3.56). Expanding for small  $\mu_O$  we note that the oxygen term

for wave normal angles near  $90^\circ$  is roughly equivalent to  $\frac{\Pi_O^2}{\Omega_O^2}$ , where  $\Pi_O$  represents the  $O^+$  ion plasma frequency.

It can be seen that there is a decrease in the growth rates when the ambient oxygen background is included. In Fig.6a the first harmonic growth rate for  $k = 9 \times 10^{-4}$  propagating at  $\psi = 89.970$  was  $\gamma = 18.15$  with a frequency of  $\omega = 31.52$  while for the same wave number in Fig.8a the growth rate was  $\gamma = 11.92$  with a frequency of  $\omega = 32.60$ . In Fig.9a the peak growth rates associated with the second harmonic have been decreased by about half compared with those of Fig.7a. The third and fourth harmonics are decreased even further. In Fig.6a-7a it can be seen that the growth rates are increasing with the increase in  $k$  whereas in Fig.10a-11a the peak growth rates are decreasing. Also, the inclusion of the oxygen eliminated the mixing that occurred in Fig.7a-7b. This is because the second, third, and fourth harmonics are being driven by the  $n=2$ ,  $n=3$ , and  $n=4$  terms of the barium expression just as in the first harmonic. Thus the frequency of the roots tends to be tied more closely to the gyroharmonics. Comparing Fig.8a-11a and Fig.8b-11b., the spread of the peak growth rates with respect to  $k$  increases for increasing gyroharmonics as well as the spread with respect to the propagation angle  $\psi$ . These roots associated with the ambient oxygen background had the maximum growth rate of  $\gamma = 16.08$  propagating at  $89.955^\circ$  for  $k = 1.2 \times 10^{-3}$  with a frequency of  $\omega = 62.55$  appearing in the second harmonic.

In comparing roots with those obtained by Xin, [1987] note that the maximum growth rate is a factor of ten larger and that the second, rather than the first,  $n=1$ , harmonic term is dominant. Also, the propagation direction of these roots is closer to  $90^\circ$  and the frequencies are closer to the cyclotron harmonics than Xin's results. We might have expected this since Crawford and Tataronis, [1965] analysis of a transverse velocity delta function distribution

showed that the first harmonic did not dominate and that the propagation occurred in frequency bands centered on the cyclotron harmonic frequency.



ZERO FREQUENCY INSTABILITY  
kpar=0.  $\rho=1\text{km}$   $z=5\text{km}$  time=1 sec  
Ba no. den.=1618. Oxy no. den.=0. (cm)<sup>-3</sup>

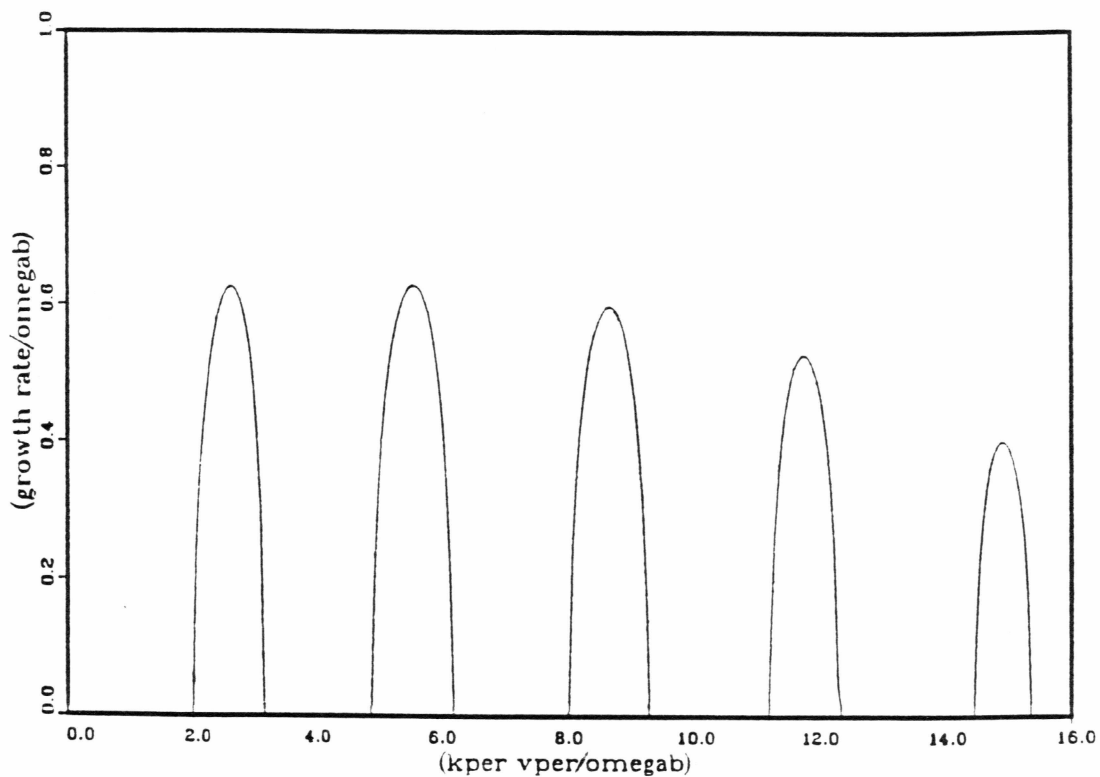


**Figure 5:** Zero frequency instabilities, perpendicular to the magnetic field, for the case with no ambient oxygen ion background

IMAGINARY PART OF ROOTS TO DISP. EQN.  
 first harmonic  $\rho=1\text{km}$   $z=5\text{km}$   $\text{time}=1\text{sec}$   
 Ba no. den.=1618. Oxy no. den.=0.  $(\text{cm})^{-3}$

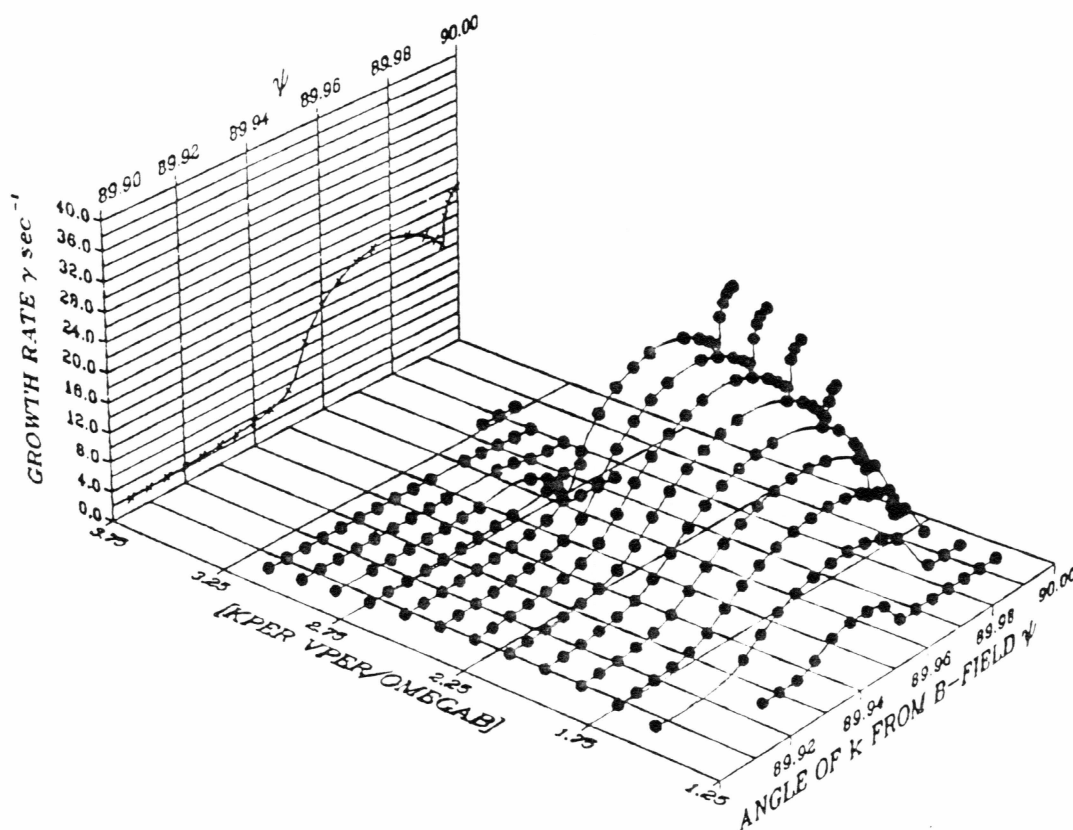


**Figure 6a:** Plasma instability (electrostatic ion cyclotron waves) corresponding to the first harmonic for the case with no ambient oxygen ion background.

REAL PART OF ROOTS TO DISP. EQN.  
 first harmonic  $\rho = 1\text{km}$   $z = 5\text{km}$   $\text{time} = 1\text{sec}$   
 $\text{Ba no. den.} = 1618$ .  $\text{Oxy no. den.} = 0$ .  $(\text{cm})^{-3}$

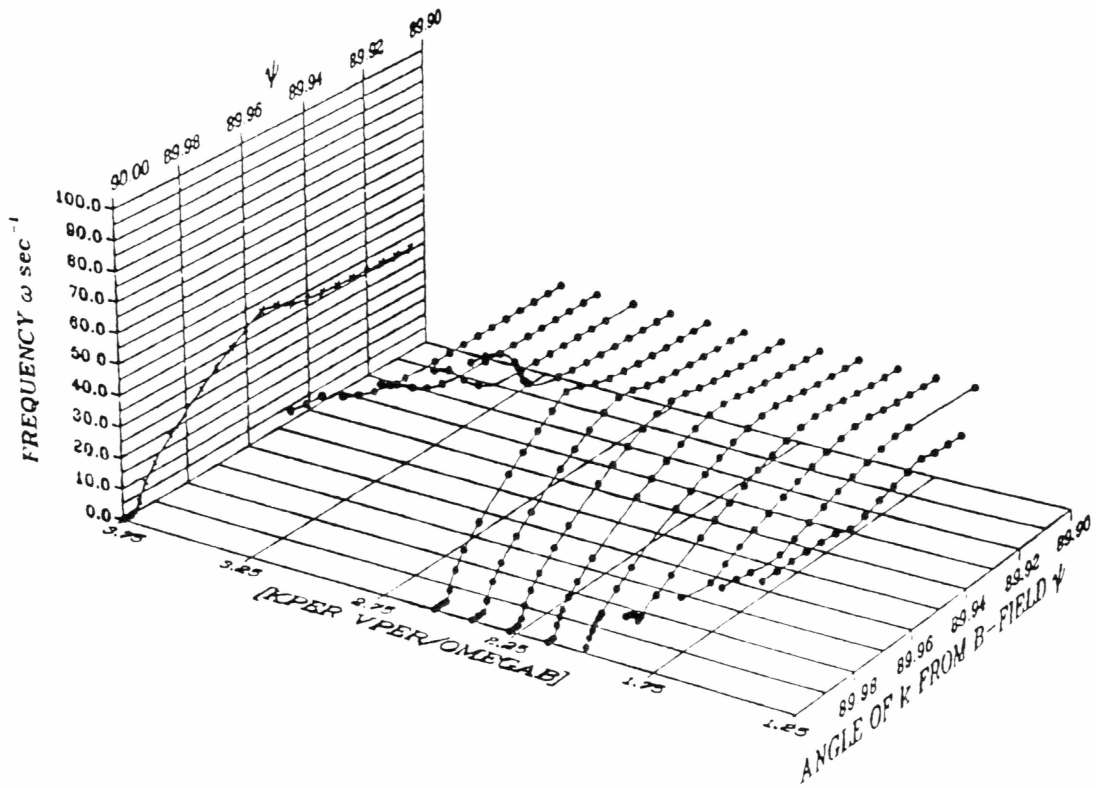
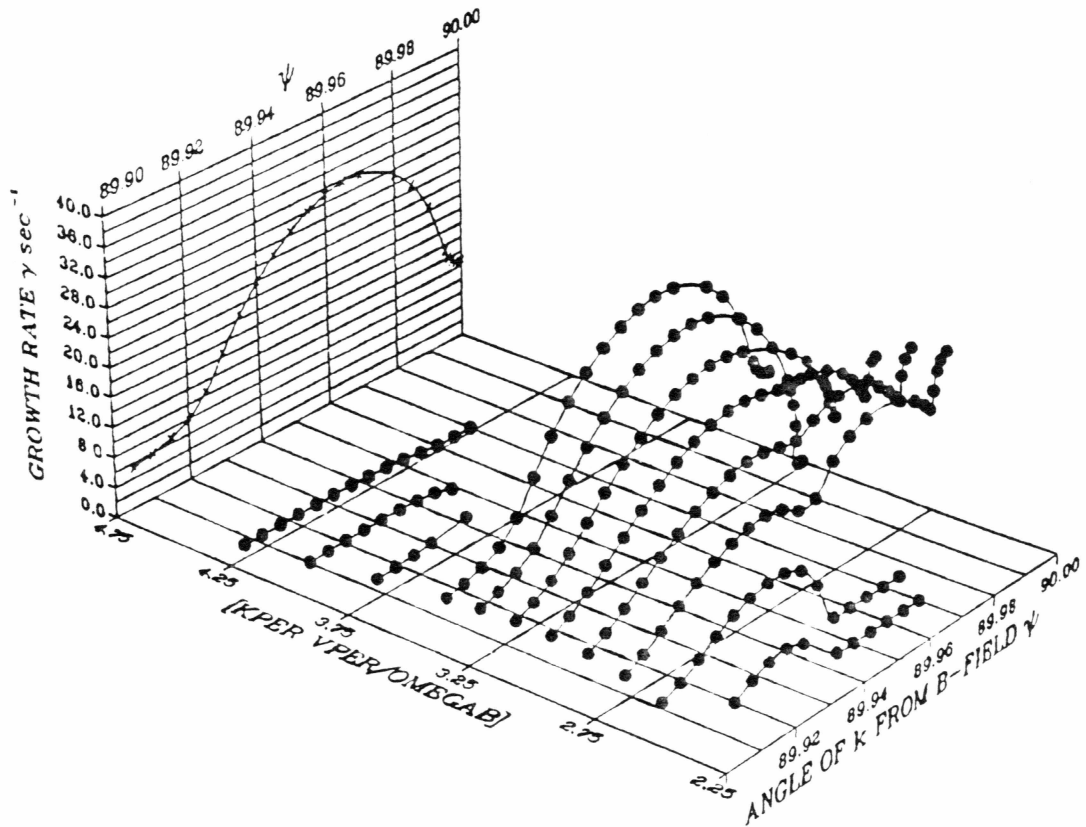


Figure 6b: Frequency associated with the first harmonic for the case with no ambient oxygen ion background

IMAGINARY PART OF ROOTS TO DISP. EQN.  
 second harmonic  $\rho=1\text{km}$   $z=5\text{km}$   $\text{time}=1\text{sec}$   
 Ba no. den.=1618. Oxy no. den.=0.  $(\text{cm})^{-3}$



**Figure 7a:** Plasma instability (electrostatic ion cyclotron waves) corresponding to the second harmonic for the case with no ambient oxygen ion background.

REAL PART OF ROOTS TO DISP. EQN.  
 second harmonic  $\rho=1\text{km}$   $z=5\text{km}$   $\text{time}=1\text{sec}$   
 Ba no. den.=1618. Oxy no. den.=0.  $(\text{cm})^{-3}$

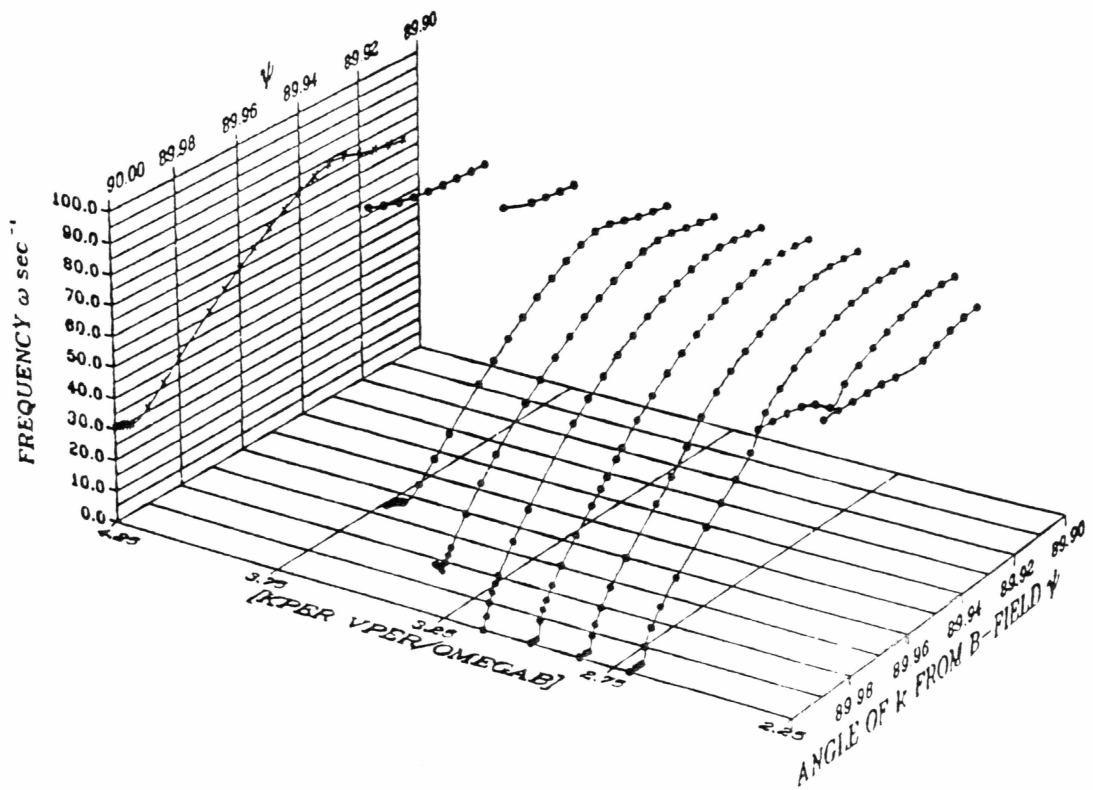


Figure 7b: Frequency associated with the second harmonic for the case with no ambient oxygen ion background

IMAGINARY PART OF ROOTS TO DISP. EQN.  
 first harmonic  $\rho=1\text{km}$   $z=5\text{km}$   $\text{time}=1\text{sec}$   
 Ba no. den.=1618. Oxy no. den.=1000.  $(\text{cm})^{-3}$

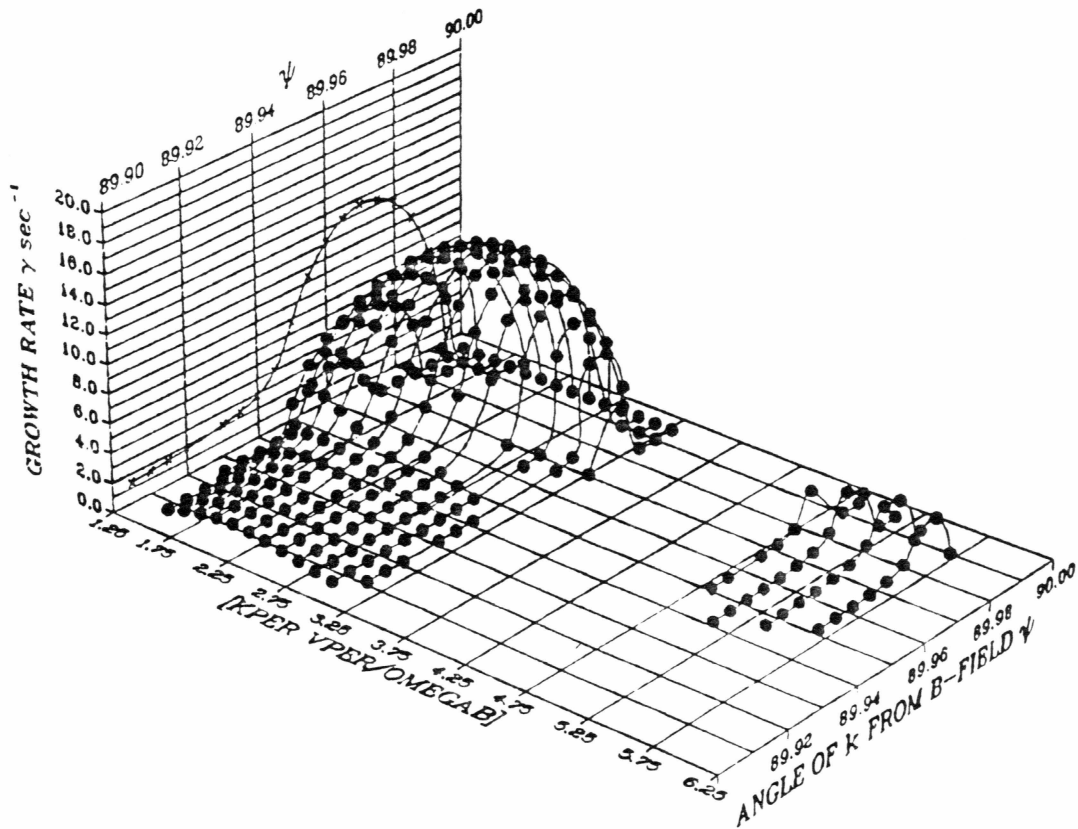


Figure 8a: Growth rates corresponding to the first harmonic for the case with an ambient oxygen ion background. The largest growth rate for the first harmonic was  $\gamma = 12.53 \text{ sec}^{-1}$  for wave number  $k = 8 \times 10^{-4} \text{ cm}^{-1}$  propagating  $89.97^\circ$  from the magnetic field with frequency  $\omega = 30.19 \text{ sec}^{-1}$ .

REAL PART OF ROOTS TO DISP. EQN.  
 first harmonic  $\rho = 1\text{km}$   $z = 5\text{km}$   $\text{time} = 1\text{sec}$   
 Ba no. den. = 1618. Oxy no. den. = 1000.  $(\text{cm})^{-3}$

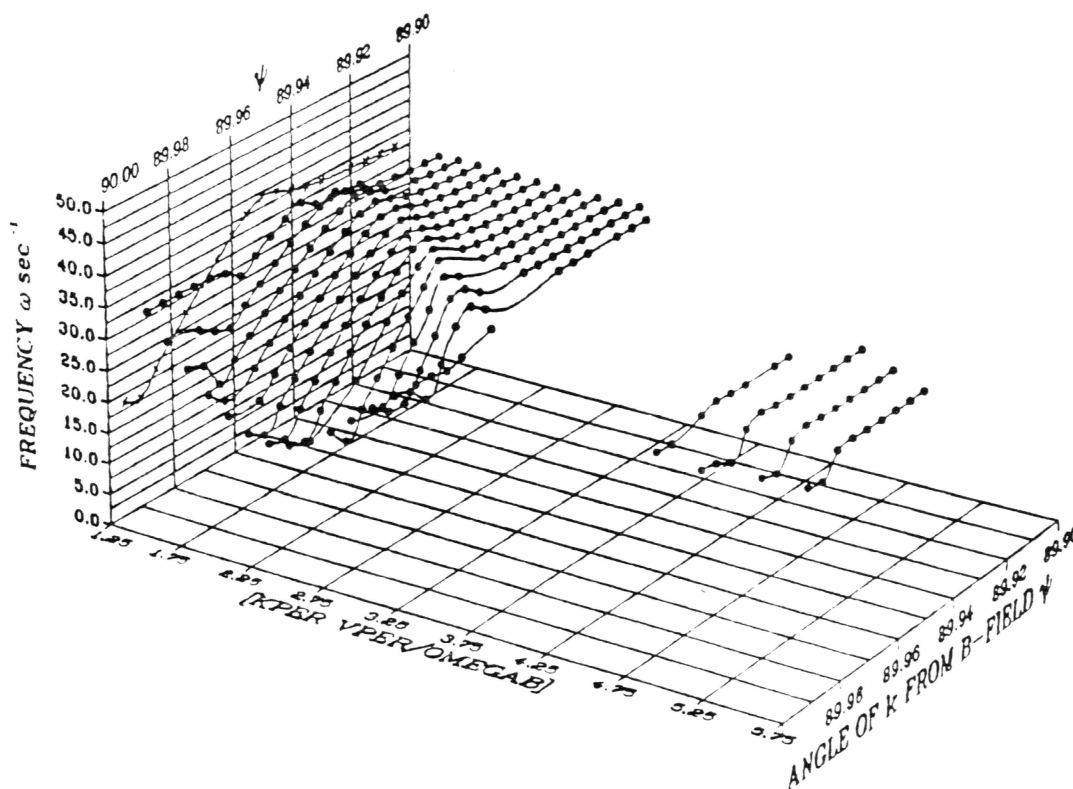
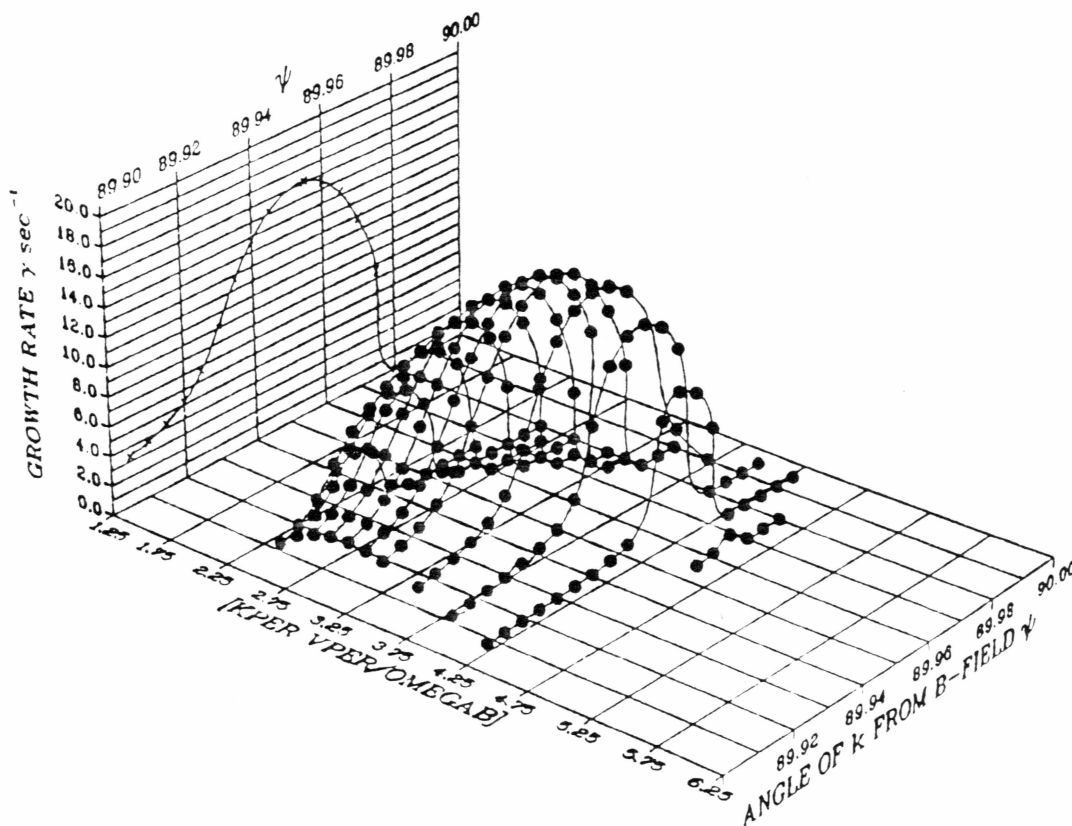


Figure 8b: Frequency associated with the first harmonic for the case with an ambient oxygen ion background

IMAGINARY PART OF ROOTS TO DISP. EQN.  
 second harmonic  $\rho=1\text{km}$   $z=5\text{km}$   $\text{time}=1\text{sec}$   
 Ba no. den.=1618. Oxy no. den.=1000.  $(\text{cm})^{-3}$



**Figure 9a:** Growth rates corresponding to the second harmonic for the case with an ambient oxygen ion background. The largest growth rate for the second harmonic was  $\gamma = 16.08 \text{ sec}^{-1}$  for wave number  $k = 1.2 \times 10^{-3} \text{ cm}^{-1}$  propagating  $89.955^\circ$  from the magnetic field with frequency  $\omega = 62.55 \text{ sec}^{-1}$ .



REAL PART OF ROOTS TO DISP. EQN.  
 second harmonic  $\rho = 1\text{km}$   $z = 5\text{km}$  time = 1sec  
 Ba no. den. = 1618. Oxy no. den. = 1000.  $(\text{cm})^{-3}$

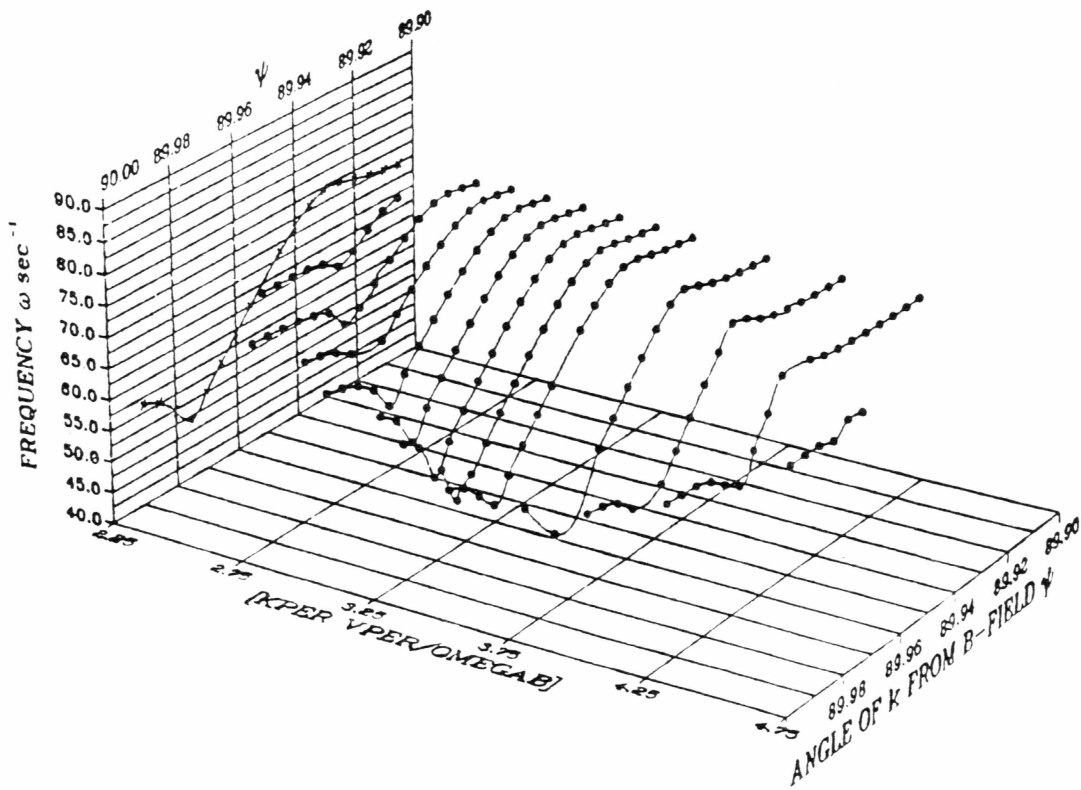


Figure 9b: Frequency associated with the second harmonic for the case with an ambient oxygen ion background

IMAGINARY PART OF ROOTS TO DISP. EQN.  
 third harmonic  $\rho=1\text{km}$   $z=5\text{km}$   $\text{time}=1\text{sec}$   
 Ba no. den.=1618. Oxy no. den.=1000.  $(\text{cm})^{-3}$

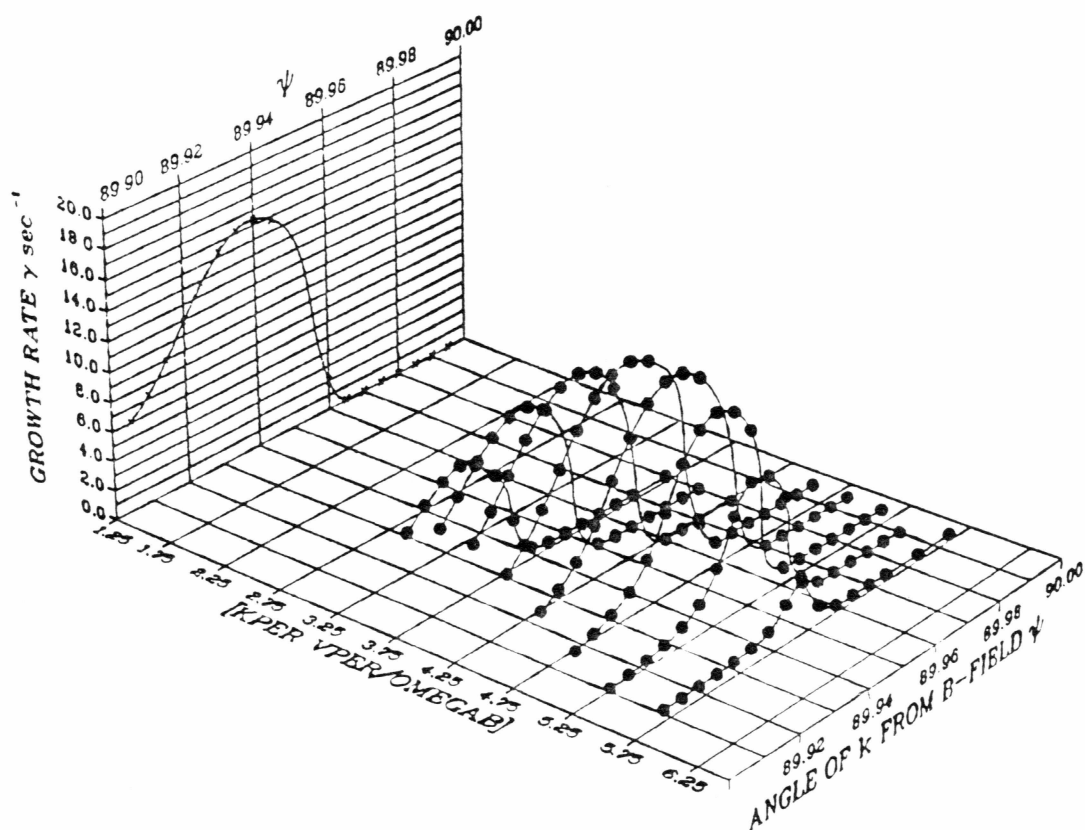


Figure 10a: Growth rates corresponding to the third harmonic for the case with an ambient oxygen ion background. The largest growth rate for the third harmonic was  $\gamma = 15.39 \text{ sec}^{-1}$  for wave number  $k = 1.6 \times 10^{-3} \text{ cm}^{-1}$  propagating  $89.94^\circ$  from the magnetic field with frequency  $\omega = 97.96 \text{ sec}^{-1}$ .

REAL PART OF ROOTS TO DISP. EQN.  
 third harmonic  $\rho = 1\text{km}$   $z = 5\text{km}$   $\text{time} = 1\text{sec}$   
 Ba no. den. = 1618. Oxy no. den. = 1000.  $(\text{cm})^{-3}$

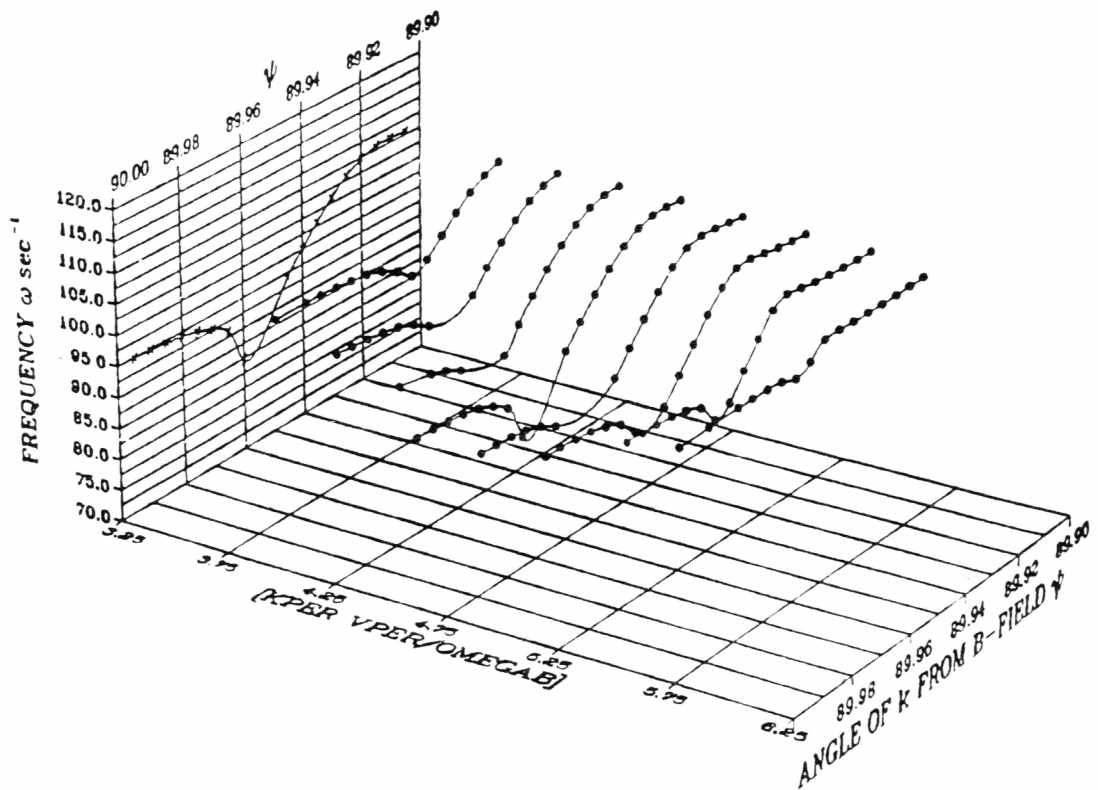
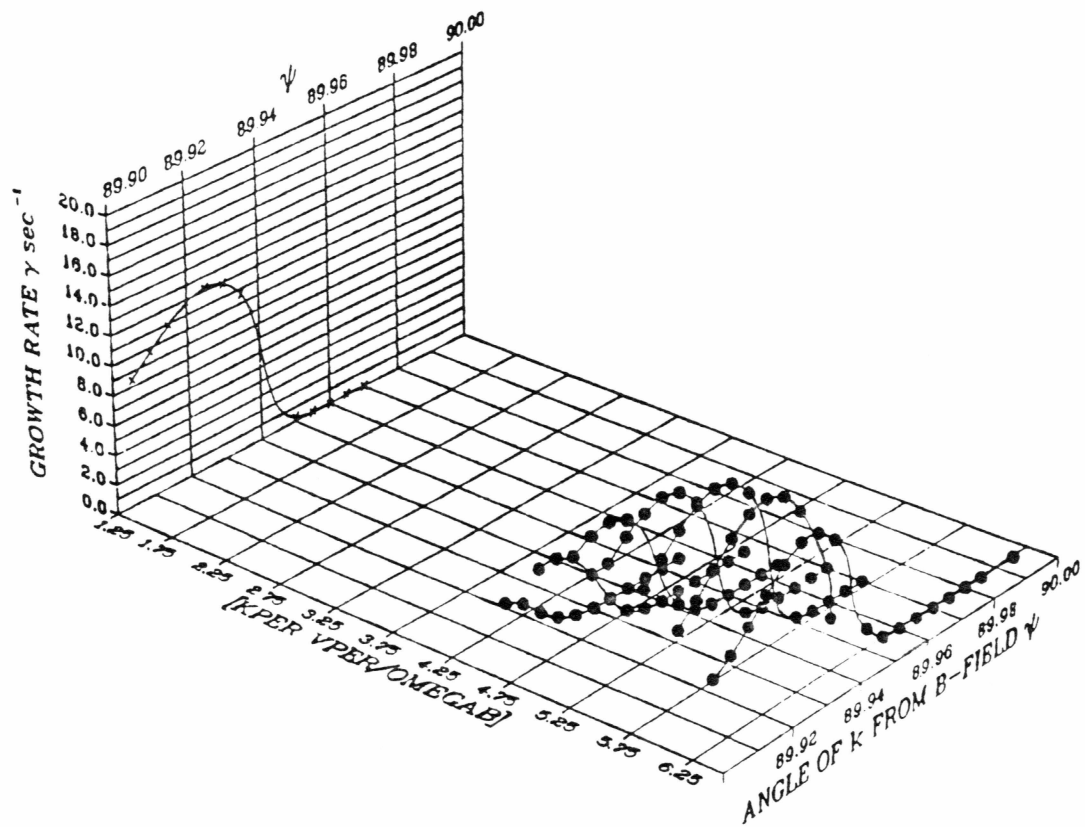


Figure 10b: Frequency associated with the third harmonic for the case with an ambient oxygen ion background

IMAGINARY PART OF ROOTS TO DISP. EQN.  
 forth harmonic  $\rho=1\text{km}$   $z=5\text{km}$  time= $1\text{sec}$   
 Ba no. den.=1618. Oxy no. den.=1000.  $(\text{cm})^{-3}$



**Figure 11a:** Growth rates corresponding to the fourth harmonic for the case with an ambient oxygen ion background. The largest growth rate for the fourth harmonic was  $\gamma = 12.22 \text{ sec}^{-1}$  for wavenumber  $k = 2.0 \times 10^{-3} \text{ cm}^{-1}$  propagating  $89.925^\circ$  from the magnetic field with frequency  $\omega = 134.45 \text{ sec}^{-1}$ .

REAL PART OF ROOTS TO DISP. EQN.  
 fourth harmonic  $\rho = 1\text{km}$   $z = 5\text{km}$  time = 1sec  
 Ba no. den. = 1618. Oxy no. den. = 1000.  $(\text{cm})^{-3}$

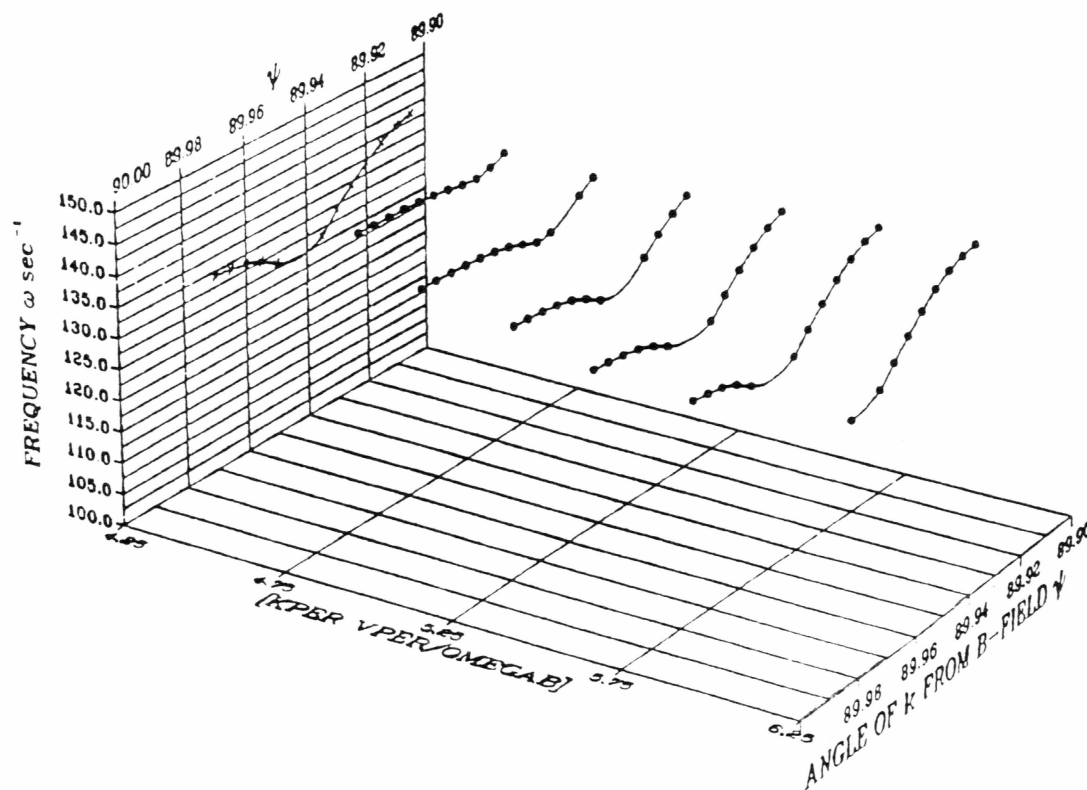


Figure 11b: Frequency associated with the fourth harmonic for the case with an ambient oxygen ion background

## Chapter 5: Conclusions

In this thesis a barium shaped charge release directed nearly parallel to the magnetic field in the  $F_2$  region of the ionosphere has been modeled for the investigation of electrostatic ion cyclotron instabilities. Established in Chapter 2 were expressions for the barium ion and the neutral number densities, where the barium ions were created from the decay of the neutral barium by the process of photoionization. The expression for the neutral barium number density was derived from the differential velocity distribution given by Stenbaek-Nielsen et al., [1984]. In Chapter 3, using the velocity distribution that was derived in Chapter 2, the dispersion relation was developed. It was then analyzed at a specific position in the barium jet and at a specific time after detonation for two cases in Chapter 4. The first case assumed no ambient oxygen ion background and in the second case an ambient oxygen ion background was assumed. In the discussion that will follow the results from Chapter 4 will be briefly stated as well as considerations how the electrostatic ion cyclotron waves would be affected by changes in the oxygen ion temperature, oxygen ion density, electron temperature, and position within the barium jet. Finally, this thesis ends by considering whether electrons can be accelerated sufficiently by electrostatic ion cyclotron waves to cause enhanced ionization of the barium neutrals.

It was found that in the case with no ambient oxygen ion background the growth rates increased with increasing wave number and frequency. The roots had considerable mixing with other modes and Crawford and Tataronis, [1965] type instabilities, which have wave normals exactly perpendicular to the magnetic field, were found.

The addition of the ambient oxygen ion background caused the decrease of the growth rates. Real roots were tied closer to the barium gyroharmonics. The Crawford and Tataro-

nis, [1965] type instabilities were eliminated, along with the mixing of the modes. Lastly, we found the second harmonic to be the dominant mode.

The introduction of the oxygen ion background had a considerable effect on the propagation of the plasma waves. In analyzing the oxygen ion term in Chapter 4 it was determined that the term was approximately  $\frac{\pi^2}{\Omega_o^2}$  for small  $\mu_o$  in eqn(3.56). Thus, the oxygen ion term was mainly dependent upon the density of the oxygen ions. Since including the oxygen ion density caused the frequency to be closer to the gyroharmonics and the growth rates to decrease, increasing the oxygen ion number density should further decrease the growth rates and tie the real roots even closer to the gyroharmonics. The oxygen term was not influenced by temperature unless  $\mu_o \approx 1$ , which corresponds to a thermal velocity of  $v_{th_o} = 3.5 \times 10^5 \text{ cm/s}$  and a temperature of  $T_o = 12000 \text{ K}$ . This temperature far exceeds the typical ion temperatures of 1000K to 2000K in the  $F_2$  region of ionosphere. Thus, the contribution of the oxygen ions is like that of a dielectric background which is only dependent upon the density. Whether increasing or decreasing the oxygen number density would cause a different harmonic to be dominant can not be said without further calculations. It is expected that increasing the electron temperature should also decrease the growth rates. The reason is that with the instabilities having parallel phase velocities greater than the electron thermal velocity, increasing the electron temperature would allow more electrons to Landau damp the wave.

In the analysis of the dispersion relation it was noted that we analyzed a case appropriate to only one point of position at a specific time in the barium jet. In order to determine what might be expected to occur at other locations we must consider the spatial dependence of the barium ion distribution. The distribution in velocity space perpendicular to

the magnetic field broadens for points close to the center of the barium ion jet. It narrows as we approach the edge of the jet. The other consideration is that the density of the barium jet decreases relative to the  $O^+$  density the farther we get away from its center. The appearance of the barium distribution stays similar to Fig.4 though the number density and the transverse velocity range can change. R.A. Dory et al., [1965] showed that absolute instabilities like that of the Crawford and Tataronis, [1965] type can be suppressed by the broadening of the transverse velocity distribution. Therefore, we might expect points approaching closer towards the center of the jet to have decreased growth rates. Thus, we would propose that the area within the barium jet where electrostatic ion cyclotron instabilities can exist may be limited to a band where the density is suitable and the barium velocity distribution has a thin enough spread in velocity. Considering the time dependence of the barium ion distribution, we would expect the area where the instabilities occur to change along with the barium jet density and velocity distribution.

Xin, [1987] examined ion cyclotron instabilities associated with the field-aligned motion of barium plasma through a background plasma of oxygen. The purpose of the study was to investigate how the instabilities may be related to the process of fast ionization reported by Hallinan, [1985]. Although the parallel phase velocity of the waves were less than the electron thermal speed, the parallel phase velocity could be Doppler shifted to speeds high enough for electrons to cause an ionization cascade. The doppler shift was associated with an  $\mathbf{E} \times \mathbf{B}$  drift generated by the finite divergence of the injected barium neutrals.

We now wish to explore the possibility of electrostatic ion cyclotron waves accelerating electrons to the ionization velocity of barium. In Chapter 4 the dominant root had a wave number of  $k = 1.2 \times 10^{-3}$  propagating at  $89.955^\circ$ . The parallel wavelength for this root,



$\lambda_{\parallel} = 67 \text{ km}$ , is much greater than the 12 km for the length of the barium jet. The longest wavelength that can likely be excited in our jet would be 24 km, which corresponds to a half wavelength. The root with the largest growth rate that has a parallel wavelength within 24 km is the fourth harmonic which has a growth rate of  $\gamma = 12.2 \text{ sec}^{-1}$ , a frequency of  $\omega = 134.5 \text{ sec}^{-1}$ , and a wave number of  $k = 2 \times 10^{-3}$  propagating at  $89.925^\circ$ . We shall investigate this wave. The largest potential that a wave can have is limited to the energy available from the cyclotron motion of the barium. Thus

$$e\phi_o < \frac{1}{2} m_{Ba} v_{\perp}^2$$

$$e\phi_o < 1.14 \times 10^{-12} \text{ ergs}$$

where  $\phi_o$  is the potential of the wave and  $v_{\perp} = 1 \text{ km/s}$ . We defined earlier

$$\phi = \phi_o \exp[i(k_{\perp} x + k_{\parallel} z - \omega t)]$$

$$\mathbf{E} = -\nabla\phi$$

So we take the maximum parallel electric field of the wave to be

$$E_{w\parallel} = \phi_o k_{\parallel}$$

where  $k_{\parallel} = 2.6 \times 10^{-6}$ . The velocity needed for an electron to ionize a barium atom is

$$v_i = \sqrt{\frac{2e\phi}{m_e}} = 1.381 \times 10^8 \text{ cm/s}$$

where the barium ionization potential  $\phi = 5.19 \text{ eV}$  [Hodgmann, 1949]. Using Newton's law we have

$$eE_{\parallel} = m_e a$$

$$a = \frac{eE_{\parallel}}{m_e} = \frac{e\phi_0 k_{\parallel}}{m_e}$$

Accelerating an electron from rest to the ionization velocity we use  $v_i = at$ , thus the time needed is

$$t = \frac{v_i}{a} = \frac{v_i m_e}{e\phi_0 k_{\parallel}} = .039 \text{ sec}$$

The distance that the particle has to travel is

$$x = \frac{1}{2}at^2 = 27 \text{ km}$$

A rough estimate of how far an electron would travel if trapped in the wave based on the size of the plasma cloud would be 10 km. It would take 3 trappings with increasing velocity increments of  $v_{inc} = 4.6 \times 10^7 \text{ cm/s}$  to accelerate an electron from rest to the ionization velocity. This corresponds to a time that the electron is trapped by the wave of  $t_p = .013 \text{ sec}$ . Since an electron trapped by a wave can undergo either acceleration or deceleration, there is an inherent randomness associated with its acceleration. The central limit theorem states that a stochastic process will reach a gaussian distribution as the number of velocity change events increases to a suitably large number [Kittel, 1958]. The standard deviation of a gaussian distribution goes as the square root of the number of iterations. Thus, a reasonable number of random trappings would be the square of the number of cumulative velocity increments it would take to reach the ionization velocity. Thus we estimate the actual time needed for the acceleration of an electron to the ionization velocity to be

$$t_{act} = N^2 t_p = .117 \text{ sec}$$

where N is the number of accelerating trappings. In a computer simulation study by Bennett, [1987] the escape of hot electrons from a region of enhanced plasma density was

investigated. It was found that electrostatic coupling of electrons to slowly moving ions significantly inhibited the escape of hot electrons. The escape time appears to depend upon the replacement of a hot electron by a cold electron. The simulation results showed that a reasonable estimate for the containment time was given by the equation

$$N(t) = N(0) \exp\left[-\frac{t}{\gamma}\right]$$

where  $N(t)$  is the number of hot particles remaining in the enhanced plasma after time  $t$  has elapsed and  $\gamma$  is the decay constant. The decay constant is described by

$$\gamma = \frac{L_1 n_1}{v_0 n_0}$$

where the subscript 1 refers to the hot region, the subscript 0 refers to the cold region, and  $L$  is the length of the enhanced region [Bennett,1987]. In our model we have  $n_0$  and  $n_1$  being the same, thus the decay constant takes the form

$$\gamma = \frac{L_1}{v_0} = \frac{L_1}{2.7 \times 10^7}$$

where  $v_0$  is the electron thermal velocity. The decay constant for the first second after detonation would have a value of  $\gamma = .044 \text{ sec}$ . This decay constant is smaller than our trapping time of .117 sec. Thus, it is unlikely that the electrostatic ion cyclotron waves would accelerate electrons to the ionization velocity. Electrons would escape well before reaching the ionization velocity and a cascade of ionization would not develop.

If the barium jet had been projected perpendicular to the magnetic field the energy available from the cyclotron motion of the barium would increase by two orders of magnitude. The wave number of the root scales as

$$\frac{k_{\perp} v_{\perp}}{\Omega_{Ba}} = 5.7$$

Using a velocity of  $v_{\perp} = 1. \times 10^6 \text{ cm/s}$  we have  $k_{\parallel} = 2.6 \times 10^{-7}$  and

$$e\phi_o < 1.14 \times 10^{-10} \text{ ergs}$$

The acceleration for an electron by the parallel electric field of the wave would be

$$a = \frac{e\phi_o k_{\parallel}}{m_e} = 3.49 \times 10^{10} \text{ cm/s}^2$$

The time for accelerating an electron from rest to the ionization velocity becomes

$$t = \frac{v_i}{a} = .00395 \text{ sec}$$

and the distance needed to obtain the ionization velocity

$$x = \frac{1}{2}at^2 = 2.7 \text{ km}$$

The time constant for the replacement of a hot electron by a cold electron for this scenario we estimate at

$$\gamma = \frac{L_1}{2.7 \times 10^7} = .011 \text{ sec}$$

where we take  $L_1 = 3 \text{ km}$  the field aligned extent of the enhancement to be less than the previous case since the electrons will traverse the width of the barium cloud. The calculations for this scenario show that larger electric fields are possible in which electrons can be accelerated to the ionization velocity in an appropriate time and distance. But, we have not considered the geometric constraints imposed on the wave. The longest parallel wavelength that can possibly propagate is twice the length of the enhanced area which is  $6 \text{ km}$ . The parallel wavelength of this case is  $\lambda_{\parallel} = 240 \text{ km}$  which is much greater. Therefore, we conclude that electrostatic ion cyclotron waves for this case would not accelerate electrons to the ionization velocity causing an ionization cascade of the barium.

In this chapter arguments have been presented on how various parameters should affect the electrostatic ion cyclotron instabilities found in Chapter 4. It was noted that the oxygen ion temperature would not affect the instability. The increasing of the oxygen ion density would have the effect of decreasing the growth rates and tying the frequencies closer to the gyroharmonics. The increasing of the electron temperature would cause a decrease in the growth rates. Considering what might be expected at other positions within the barium jet, it was concluded that the instability would be confined to a band where the density is suitable and the transverse velocity distribution has a thin enough spread in velocity. Calculations were done to determine if these instabilities could cause an ionization cascade of the barium. It was determined that, for the instabilities considered, an ionization cascade would not develop for the barium jet when it is injected in a direction parallel to the magnetic field. We then considered the situation where the injected barium jet was directed perpendicular to the magnetic field. In this case it was determined that the instability would not be present due to the geometric considerations of the parallel wavelength of the instability being much greater than the barium jet's width. So, these waves would not cause a cascade of ionization to occur for a barium jet injected in a direction perpendicular to the magnetic field nor help contribute to Alfvén's critical velocity mechanism. The author wishes to note that computational considerations allowed only a particular point of position at a specific time to be evaluated. It was not possible to obtain the maximum growth rate associated with the barium jet. The arguments presented seem to dictate that the electrostatic ion cyclotron instabilities within the barium jet would not promote an enhanced ionization.

## References

- Abramowitz, M., and I. A. Stegun, editors, *Handbook of Mathematical Functions*, National Bureau of Standards, 1972.
- Alfven, H., *On the Origin of the Solar System*, Oxford at the Clarendon Press, London, 1954.
- Banks, P. M., and G. Kockarts, *Aeronomy*, Academic Press, New York, 1973.
- Bennett, M. J., The computer simulation of electrons escaping from a region of hot plasma, *Report Contributed to 1987 Summer Intern Program at the Geophysical Institute*, University of Alaska, Edited by D. Swift, 1987.
- Crawford, F. W. and J. A. Tataronis, Absolute instabilities of perpendicularly propagating cyclotron harmonic plasma waves, *J. Geophys. Res.*, *36*, p. 2930-2934, 1965.
- Danielsson, L. and N. Brenning, Experiment on the interaction between a plasma and a neutral gas. II, *Phys. Fluids*, *18*, p. 661-671, 1975.
- Dory, R. A., G. E. Guest, and E. H. Harris, Unstable electrostatic plasma waves propagating perpendicular to a magnetic field, *Phys. Rev. Letters*, *14*, P.131-133, 1965.
- Drapatz, S. W., The radiative transfer problem in freely expanding gaseous clouds and its application to barium cloud experiments, *Planet. Space Sci.*, *20*, p. 663-682, 1972.
- Haerendel, G., Alfven's critical effect tested in space, *Z. Naturforsch. A*, *37*, p. 1042, 1982.
- Hallinan, T. J., Rapid ionization of barium injection parallel to B, *EOS*, *66*, p.1042, 1985.
- Hallinan, T. J., Observed rate of ionization in shaped-charge releases of barium in the ionosphere, *J. Geophys. Res.*, *93*, p. 8705-8712, 1988.

- Hasegawa, A., *Plasma Instabilities and Nonlinear Effects*, Springer-Verlag, 1975.
- Hodgmann, C. D., *Handbook of Chemistry and Physics*, Chemical Rubber Company Publishing, Cleveland, 1949.
- Jackson, J. D., *Classical Electrodynamics*, John Wiley and Sons, New York, 1975.
- Kindel, J. M. and C. F. Kennel, Topside current instabilities, *J. Geophys. Rev.*, 76, p. 3055-3078, 1971.
- Kittel, C., *Elementary Statistical Physics*, John Wiley and Sons, New York, 1958.
- Mobius, E., Critical velocity experiments in space, Symposium at Alpbach, 24-28 May 1983, *Eur. Space Agency Publ., ESA SP-195*, p. 215, 1983.
- Nicholson, D. R., *Introduction to Plasma Theory*, John Wiley and Sons, New York, 1983.
- Stenbaek-Nielsen, H. C., T. J. Hallinan, E. M. Wescott, and H. Foppl, Acceleration of barium ions near 8000km above an aurora, *J. Geophys. Rev.*, 89, p. 10788-10800, 1984.
- Wescott, E. M., E. P. Rieger, H. C. Stenbaek-Nielsen, T. N. Davis, H. M. Peek, and P. J. Bottoms, The L=6.7 quiet time barium shaped charge injection experiment "Chachalaca", *J. Geophys. Rev.*, 80, p. 2738-2744, 1975a.
- Wescott, E. M., H. C. Stenbaek-Nielsen, T. N. Davis, W. B. Murcray, H. M. Peek, and P. J. Bottoms, The L=6.6 Oosik barium plasma injection experiment and magnetic storm on March 7, 1972, *J. Geophys. Rev.*, 80, p. 951-967, 1975b.
- Wescott, E. M., H. C. Stenbaek-Nielsen, T. Hallinan, H. Foppl, and A. Valenzuela, Star of Lima: Overview and optical diagnostics of a barium Alfvén critical velocity experiment, *J. Geophys. Rev.*, 91, p. 9923-9931, 1986a.

- Wescott, E. M., H. C. Stenbaek-Nielsen, T. Hallinan, H. Foppl, and A. Valenzuela, Star of Condor: A strontium critical velocity experiment, Peru, 1983, *J. Geophys. Rev.*, 91, p. 9933-9938, 1986b.
- Xin, W., An anomalous process of fast ionization of a barium shaped charge release, *M.S. Thesis*, University of Alaska, 1987.